ISBN 978-82-326-1798-2 (printed version)
ISBN 978-82-326-1799-9 (electronic version)
ISSN 1503-8181

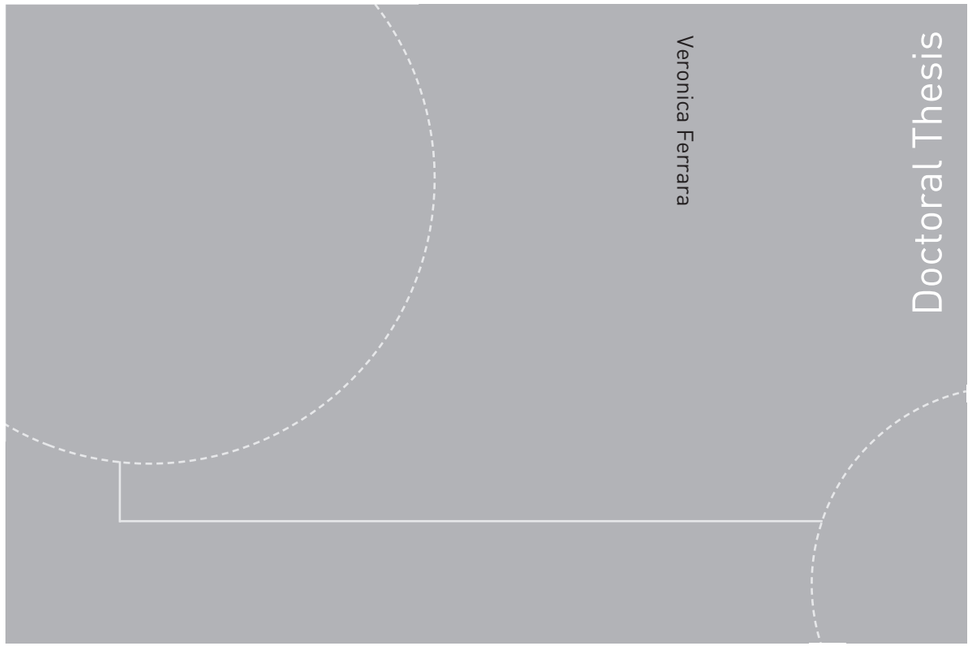

Doctoral theses at NTNU, 2016:230

Veronica Ferrara

Wet Gas Compressors - Stability and Range

NTNU
Norwegian University of
Science and Technology
Faculty of Engineering
Science and Technology
Department of Energy and Process Engineering

NTNU
Norwegian University of
Science and Technology

Doctoral theses at NTNU, 2016:230

NTNU

NTNU
Norwegian University of
Science and Technology

Veronica Ferrara

Wet Gas Compressors - Stability and Range

Thesis for the degree of Philosophiae Doctor

Trondheim, September 2016

Norwegian University of Science and Technology
Faculty of Engineering Science and Technology
Department of Energy and Process Engineering

NTNU
Norwegian University of
Science and Technology

NTNU
Norwegian University of Science and Technology

Thesis for the degree of Philosophiae Doctor

Faculty of Engineering Science and Technology
Department of Energy and Process Engineering

© Veronica Ferrara

ISBN 978-82-326-1798-2 (printed version)
ISBN 978-82-326-1799-9 (electronic version)
ISSN 1503-8181

Doctoral theses at NTNU, 2016:230

Printed by Skipnes Kommunikasjon as

Abstract

The oil and gas industry is a large user of turbomachinery. The demand for oil and gas is consistently growing, and changing market conditions require innovative solutions. Operation and optimization of turbomachinery in a variety of applications is therefore of great interest. Moreover, potentially extreme environmental procedures mean that innovative design and operational attributes must be used.

The development and implementation of new subsea technology is an important focus area to increase petroleum production and recovery from existing fields. The technology will contribute to the exploitation of small and remote fields and access to fields in very deep water. A traditional centrifugal compressor may not be applicable for wet gas compression, because the liquid may cause mechanical damage due to erosion and corrosion of the compressor components; in addition, the design is not optimized for multiphase flow. In this research, particular emphasis is given to the wet gas compressor as a more fundamental knowledge of the impact of liquid is essential with regard to the understanding of aerodynamic and fluid dynamic compressor behaviour. It is also of vital importance to identify the mechanisms leading to unsteadiness, like surge and rotating stall. A key element is the investigation of the machine performance and working range when a liquid phase is present.

In the present work, attention has been given to the experimental validation of an advanced facility, equipped with special windows designed for flow inspection. The experimental tests were performed on an air-water multiphase open-loop test rig, which consists of a single-stage centrifugal compressor, with a standard three-dimensional impeller that was tested in dry and multiphase conditions.

The main objective of this research is the study of the stability and the range of the wet gas compressor at a low mass flow rate. Focus of interest is on the effect of the presence of a liquid phase. Thus the performance evaluation from dry to wet operating conditions is fundamental. Moreover the study of the flow path inside the impeller and the diffuser has great importance in order to clarify the impact of the liquid. In this case the visualization of the fluid has a central role. The analysis of the working range has been supplemented by the investigation at off–design conditions, in particular in the area characterized by low mass flow rate. An accurate examination of the dynamic pressure trends from dry to wet working conditions is carried out.

The results show the performance deterioration owing to the content of liquid with respect to dry working conditions. However the presence of a liquid has a positive influence on the machine stability and operating range. Through a fast Fourier transform analysis, the stabilizing effect on instabilities onset is highlighted, compared to normal operations. In addition, the flow evolution inside the impeller and diffuser is studied. The main flow patterns, typical of a centrifugal compressor, are revealed also in wet conditions: the impeller flow presents a jet-wake structure, while in the diffuser a logarithmic spiral path is observed. Also the characteristic behaviour, like reverse flow that creates a “doughnut” formation, towards the suction pipe, is documented.

The outcomes that improve the knowledge about the wet gas compressor are a baseline to define a method in order to conduct multiphase tests and provide a starting point to design a wet tolerant system.

Nomenclature

b	Width [mm]
BPF	Blade passing frequency [Hz]
c	Absolute velocity [m/s]
CFD	Computational fluid dynamics
D	Diameter [mm]
FFT	Fast Fourier transform
FT	Flow transmitter
GMF	Gas mass fraction [-]
GVF	Gas volume fraction [-]
h	Enthalpy [kJ/kg]
LMF	Liquid mass fraction [-]
LVF	Liquid volume fraction [-]
$\dot{m}$	Mass flow [kg/s]
Mu	Mach number [-]
NTNU	Norwegian University of Science and Technology
p	Pressure [Pa]
P	Power [W]
PR	Pressure ratio [-]
PT	Pressure transmitter
r	Radius [m]
R_n	Curvature
Ro	Rossby number [-]
RPM	Speed [rpm]
T	Torque [Nm]
TT	Temperature transmitter
u	Impeller peripheral velocity [m/s]
w	Relative velocity [m/s]
W	Work [J]
α	Absolute flow angle [°]
β	Blade angle [°]
ϱ	Density [kg/m^3]
η	Polytropic efficiency [-]
τ	Work coefficient [-]
φ	Flow coefficient [-]
ω	Rotational speed [rad/s]

Subscripts

1	impeller inlet section
2	impeller outlet section
3	diffuser outlet section
eff_mech	effective mechanical
g	Gas
l	Liquid
mech	mechanical
pol	polytropic
r	radial component
u	tangential component

1. Introduction

Wet gas compression is a new technology which the oil and gas industry has focused on recently. Research in this field is of considerable interest, since a better understanding of mechanisms which occur operating from dry to wet conditions is vital. In this thesis the author makes her contribution to increase knowledge, summarizing the outcomes from experimental tests that were planned and performed during her PhD programme at the Norwegian University of Science and Technology (NTNU).

Scope of the work

The development of wet gas compression requires investigations on the effect of the presence of a liquid phase, handled by a centrifugal compressor. Consequently, the machine performance and behaviour have a great importance, and experimental results are needed to improve the design and develop models for predicting compressor performance and unsteady control methods under wet conditions.

The main objective of this work is to analyse the stability and range of a centrifugal compressor at off-design operating conditions, with particular regard to unstable phenomena, like stall and surge. Key points are

- Establish dry and wet compressor performance by post-processing measurements from experimental tests. Identifying stall and surge conditions during operation with the presence of a liquid phase and comparing them with fundamental literature results.

- Visualize the flow mechanisms, defining the behaviour inside the impeller and diffuser at low inlet flow, close to surge condition. Of specific interest is determining the impeller flow regime, fluid accumulation and back flow phenomena, with particular regard to the inlet tip area.

- Document the flow shift in correspondence with impeller discharge/diffuser inlet section and investigate the interactions between the machine components. In addition, the diffuser flow path identification is a fundamental issue.

- Left limit investigation, in order to define the working range of the machine and understand the effect of the liquid presence on the unsteadiness margin. The attention is focused also on documentation of instability characteristic frequencies.

Contribution

The fundamental contributions of this work are collected in four papers that were presented at the main sector conferences:

Paper I is based on experimental test campaign. Test activity was planned and performed by the author; data analysis and post processing have been accomplished by the author as well.

Paper II is based on experimental test campaign, performed by the author and a master's student, Tore Eikevåg. Test procedure was defined by the author, as well as accomplishment of data analysis. The images presented in the paper were edited by the student.

Paper III is based on experimental test campaign, performed by the author together with master's students, Håvard Skjefstad and Sindre Garpestad Tønnesen. Test procedure, experimental activity and data analysis were specified by the author.

Paper IV is based on preliminary test campaign achieved by the author, in collaboration with GE Oil and Gas. Test activity and post processing have been performed by the author. The "OEM's predictive mode validation" section is not author's contribution to the paper.

Limitations

This study has been performed with a standard three-dimensional impeller. During the multiphase investigations, carried out at an NTNU laboratory, an air-water mixture has been employed, although in normal operation hydrocarbon is the working fluid. The liquid-gas density ratio differs significantly, in particular in a real plant the value of this coefficient is less than the experimental tests.

Thesis outline

This thesis consists of a wide experimental campaign; attention has been focused on flow visualization and performance tests, involving transient and working range analysis.

Chapter 1 The scope of work is introduced.

Chapter 2 A general overview about centrifugal compressor theory is given. The principal subjects are flow pattern, with particular regard to jet-wake structure, aerodynamic stability and instability. Connections with multiphase flow are discussed for each topic. In addition an introduction related to wet gas compression is proposed.

Chapter 3 The test facility and installed instrumentation are described.

Chapter 4 Test campaigns with related text matrix are documented. Results from experimental campaigns are reported. Compressor performance, flow visualization, left limit and erosion tests are analysed.

Chapter 5 Conclusion

References

Appendix Author' selected papers are attached

2. Centrifugal compressor basics: from dry to wet conditions

This chapter reviews theory about centrifugal compressors, with particular regard to performance and flow velocity. Attention is focused on impellers with backward-curved blades and vaneless diffusers, since components with the present characteristics are installed in the test facility which is employed in the experimental tests, as clarified in the following chapters.

The typical flow patterns are described by studying the literature. Focusing on the fundamentals relating to secondary flows and machine components interactions, a direct link with multiphase fluid is given. From dry to wet operating conditions, main and secondary stream flows are visualized, so a summary of basics is useful to pinpoint the similarities.

The author has completed an in-depth analysis relating to unsteadiness detection by frequency investigation. Systems applied in dry conditions represent feasible methods also moving towards wet operations.

Overview and performance

A centrifugal compressor is a dynamic machine where the pressure rise is achieved by a dynamic transfer of energy to a continuous flow of stream.

A typical single-stage configuration consists of a rotating impeller, a diffuser and a volute. Fig. 1 illustrates the cross-section of the NTNU centrifugal compressor stage.

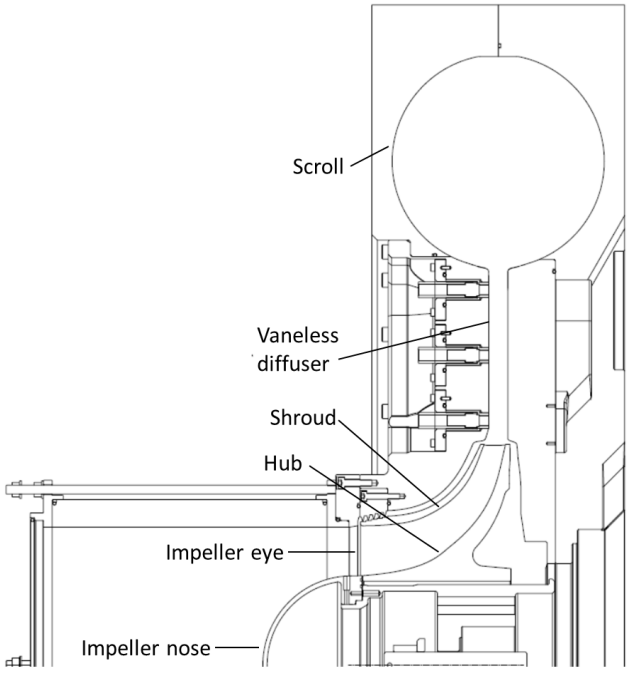

Fig. 1: Centrifugal compressor stage. Cross-section of NTNU test facility.

Taking into account an external reference system to the compressor, the rotor has a velocity u, while the fluid enters to the impeller with an absolute velocity c. On the contrary, in a coordinate system integral with the rotating apparatus, the rotor is still and the fluid has a relative velocity w. Through a vector representation, refer to Fig. 2, the velocities relation result in

$$c = w + u$$

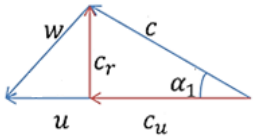

Fig. 2: Velocity triangle

The absolute velocity, c, can be split along the radial, c_r, and the tangential, c_u, components.

Impeller

The impeller is responsible to increase the energy content of the fluid by raising its velocity. Generally the air enters in the axial direction from the impeller eye and is whirled outward by the blades. Taking into examination the impeller inlet and outlet sections. indicated by subscripts 1 and 2, respectively, it is possible to obtain through the equation of balance of momentum

$$T = \dot{m}(r_2 c_{2u} - r_1 c_{1u}) \qquad \text{Eq. 1}$$

where T is the torque supplied by the impeller to the fluid.

Introducing the peripheral speed (or blade speed) $u = \omega r$, the work transferred by the blades per mass unit of fluid processed can be expressed as

$$W = \frac{T\omega}{\dot{m}} = u_2 c_{2u} - u_1 c_{1u} \qquad \text{Eq. 2}$$

The first principle of thermodynamics establishes the specific work, for adiabatic flow, is equal to the variation in total enthalpy. Eq. 2 can be revised in terms of total velocities, obtaining

$$\Delta h = \frac{u_2^2 - u_1^2}{2} + \frac{w_1^2 - w_2^2}{2} + \frac{c_2^2 - c_1^2}{2} \qquad \text{Eq. 3}$$

Eq. 2 and Eq. 3 are the two forms of the Euler turbomachinery equation. The latter describes the energy transfer terms, in particular the first two terms show the static, while the third gives the dynamic enthalpy rise. The study of these energy interactions requires the analysis of velocities, usually carried out by speed triangles.

Assuming an axial entry (α_1= 90°) the tangential component of the absolute velocity $c_{1u} = c_1 \cos \alpha_1$ is zero, consequently the work done on the fluid is $\Delta h = u_2 c_{2u}$. The inlet triangle is sketched in Fig. 3.

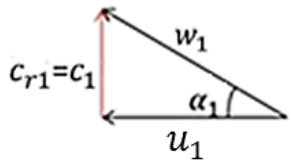

Fig. 3: Velocity triangle at impeller inlet

Considering a fluid particle, the acceleration is expressed by

$$\frac{dc}{dt} = \frac{dw}{dt} + \omega \times (\omega \times r) + 2\omega \times w \qquad \text{Eq. 4}$$

The first term in Eq. 4 is the relative acceleration, the second the centrifugal acceleration while the last the Coriolis acceleration. Potential energy is associated with the centrifugal acceleration by varying the radius, and can be expressed as $\frac{u_2^2-u_1^2}{2}$. Rearranging the energy equation, one obtains

$$h_2 - h_1 = \frac{u_2^2-u_1^2}{2} - \frac{w_2^2-w_1^2}{2} \qquad \text{Eq. 5}$$

Where $h + \frac{w^2}{2} - \frac{u^2}{2}$ is defined rothalpy. So in a rotor this quantity is constant, and it is evident the enthalpy rise inside the impeller is due to two contributions: the centrifugal effect and the deceleration of the relative flow. The former is loss free, because it is unconnected with the flow process, while the losses affect the second term in Eq. 5. They are directly related to the relative flow deceleration and not to the overall change in static enthalpy.

Diffuser

The diffuser decelerates the flow leaving the impeller, normally with high absolute velocity and inclined at a large angle to the radial direction. Its purpose is to recover the kinetic energy as much as possible with a minimum loss in total pressure. It should be taken into account that diffusion could be affected by boundary layer separation from the wall if the process is too rapid. On the contrary, if the deceleration is too low, the fluid friction losses become excessive.

As for the impeller, it is possible to give a velocity representation of the fluid at the diffuser section inlet. In Fig. 4 a characteristic situation for backward-curved vane is depicted: the absolute tangential velocity increases with the reduction of the flow rate, the absolute radial component drops accordingly.

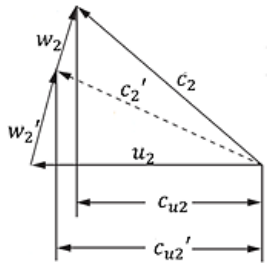

Fig. 4: Velocity triangle at diffuser inlet

Fig. 5 represents the particle trajectories through a vaneless diffuser at the design (Fig. 5a) and part-load (Fig. 5b) conditions, respectively. Reducing the mass flow rate in

correspondence with the impeller inlet and keeping the rotational speed constant, a decrease in the relative velocity, w_2, is observed. The length of the spiral flow path increases accordingly, as shown in Fig. 5b. If the flow trajectory is extended beyond the design path, the momentum at the diffuser walls is excessively dissipated, reducing the diffuser efficiency, since a proportionately smaller amount of velocity is converted to pressure rise.

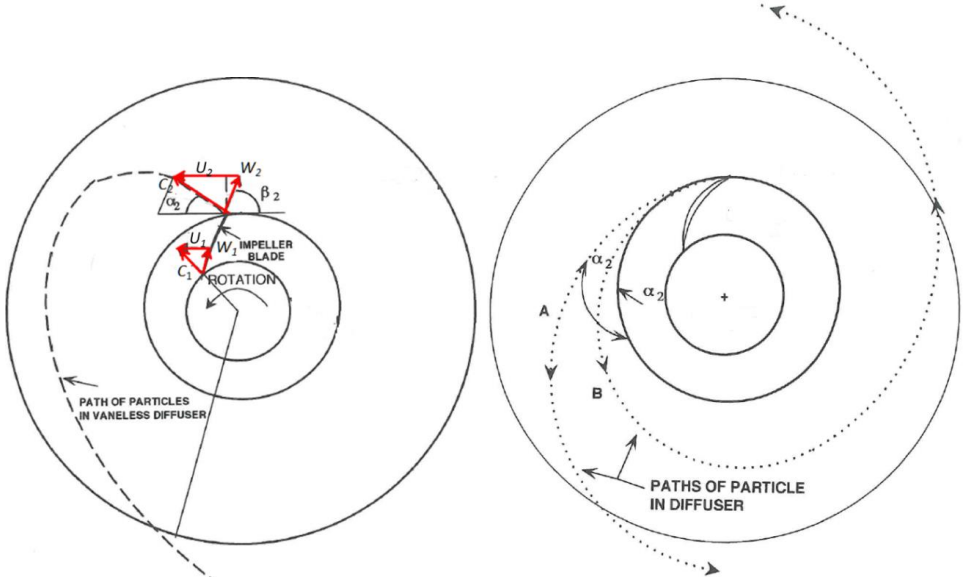

(a) (b)

Fig. 5: Flow trajectory in a vaneless diffuser; (a) design condition, (b) part-load condition

As usual with any machine, the quantity of energy absorbed by the compressor cannot be entirely converted into a pressure increment because of dissipation phenomena of various kinds involving the machine as a whole. Inevitable losses cause a significant difference between theoretical and actual output. The factors that determine and influence machine performance are due to friction and incidence. The friction dissipations are mainly produced by wall friction, fluid shear and flow separation. Fig. 6 depicts the graphical interpretation of head drop, associating the reduction of the theoretical curve for backward blades to all losses. The energy is diminished by the dissipation associated with pressure drop due to friction and incidence (shock losses), both expressed by parabolic equations.

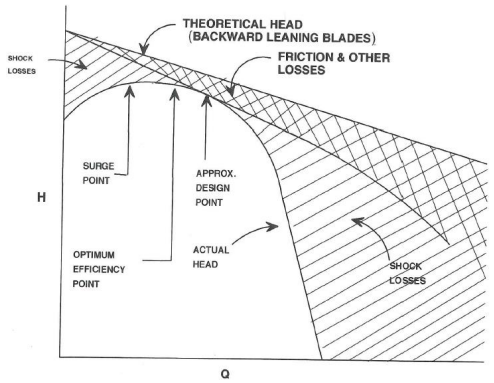

Fig. 6: Typical compressor head losses for backward blades [1]

However the actual head curve shape is vital for compressor stability, as depicted in Fig. 7, in which a comparison on the effect of different impeller blade angle appears. It should be noted the lower curve presents the most gradual variance in steepness on the left-hand side of the characteristic. This represents the highly desirable condition for the stability.

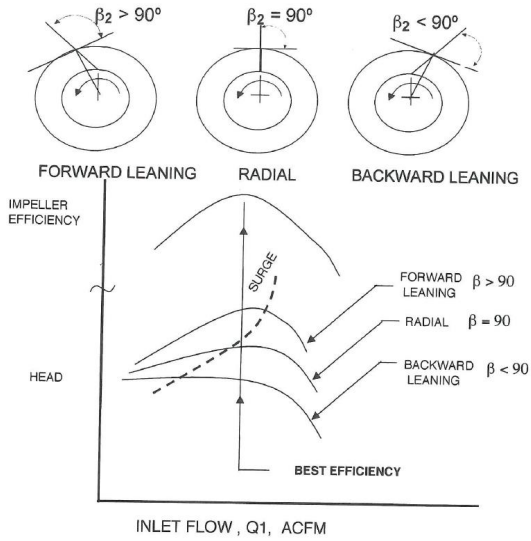

Fig. 7: Effect of blade angle on compressor stability [1]

Multiphase fluid

Fundamental equations, expressing parameters employed in the following chapter for performance analysis are given below. A basic coefficient, used in wet gas compression to characterize the flow composition is the gas mass fraction (GMF), calculated as

$$GMF = \frac{\dot{m}_g}{\dot{m}_g + \dot{m}_l} \quad \text{Eq. 6}$$

And the liquid mass fraction (LMF)

$$LMF = \frac{\dot{m}_l}{\dot{m}_g + \dot{m}_l} \quad \text{Eq. 7}$$

The polytropic efficiency, η_p, is evaluated as:

$$\eta_p = \frac{\Delta h_{pol}}{\Delta h_{eff\_mech}} \quad \text{Eq. 8}$$

with

$$\Delta h_{eff\_mech} = \frac{W_{eff\_mech}}{\dot{m}_g + \dot{m}_l} \quad \text{Eq. 9}$$

and

$$\Delta h_{pol} = LMF \, \frac{p_{out} - p_{in}}{\rho_l} + (1 - LMF) \, \Delta h_{pol\_g} \quad \text{Eq. 10}$$

From previous formulas, it emerges that polytropic efficiency is computed by the energy input from the shaft. So inaccuracy of temperature measurement due to the presence of a liquid phase has a minor effect on the efficiency evaluation. Moreover in [2], it arises from a regression analysis with variables that mainly affect the performance compressor parameters under wet conditions. These are the liquid mass fraction and the liquid volume fraction (LVF).

A dimensionless coefficient, inherent characteristic exclusively of the impeller, is the work coefficient, τ, calculated as:

$$\tau = \frac{\Delta h_{eff\_mech}}{u_2^2} \qquad \text{Eq. 11}$$

It is useful to define also the flow coefficient, a no dimensional parameter is mainly used for impeller design and performance evaluation:

$$\varphi = \frac{4\dot{Q}_1}{\pi D_2^2 u_2} \qquad \text{Eq. 12}$$

Flow patterns

The flow in a centrifugal compressor is three-dimensional and the impeller and diffuser behaviour are quite different. Mostly because of a change of flow direction inside the impeller: the flow enters in the axial direction and leaves through the radial path, causing a velocity variation from the hub to the shroud as well.

A complete flow analysis is a three-dimensional application, originally proposed by Wu (1952) and widely employed in numerical simulations by solving the compressible Navier-Stokes equations or considering the flow as inviscid and applying the Euler code, in the compressible form. Due to the actual CFD limitation, it is common practice to refer to a quasi-three-dimensional analysis. This approach uses two interacting 2D surface, depicted in Fig. 8: one in the meridional plane (hub-to-shroud) and the other in the stream surface (blade-to-blade)

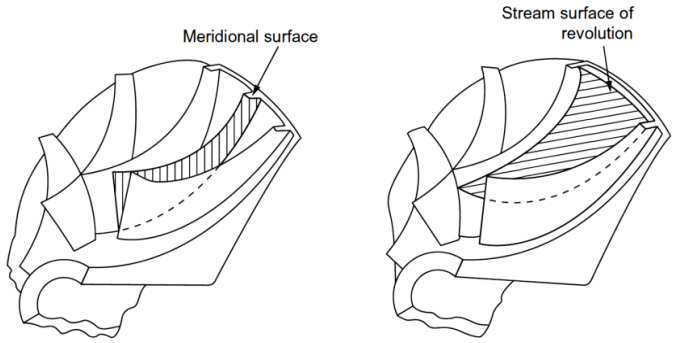

Fig. 8: Two-dimensional surfaces for flow analysis [3]

This formulation is valid for inviscid flow in a steady state condition, consequently some errors and inaccuracies arise, in particular produced by the neglected viscous effects. In a specific situation, it is possible to apply a one-dimensional analysis. In this case the flow is studied in a mean stream surface, implementing the basic mass, momentum and energy equations and empirical loss models.

Dry gas

The most complex component in a centrifugal compressor, concerning the flow analysis, is the impeller. A centrifugal impeller presents a strong curvature both in the meridional and in the blade-to-blade plane. In addition the vanes are long in relation to the cross-sectional area, causing high non-uniform flow. Dean and Senoo [4] were the first to propose a model explaining the flow separation, developing a theory based on a jet-wake pattern, in Fig. 9: two areas characterized by different stagnation pressure and, consequently, diverse relative velocities. The phenomenon occurs in correspondence with the impeller discharge, because of a reversible pressure work transfer between the various regions of the flow.

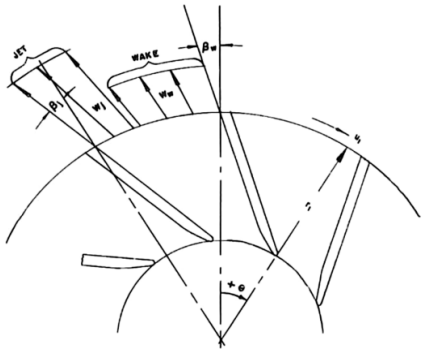

Fig. 9: Jet-wake flow pattern as described by Dean and Senoo (1976) [4]

Eckardt confirmed Dean and Senoo's idea and provided the most complete explanation of the flow patter inside the impeller. Collecting numerous laser velocimetry measurements (Fig. 10), Eckardt [5], gave a description of the jet-wake structures in a radial impeller, recognizing a flow separation in the shroud-suction side corner of the channel. The governing foundation of the phenomenon is the turbulence stabilization of the boundary layer, because of streamline curvature and rotation effects.

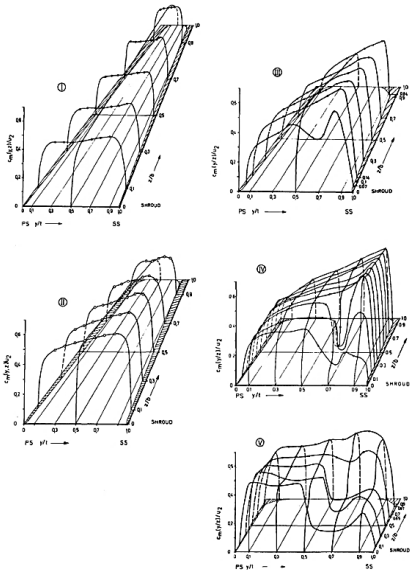

Fig. 10: Velocity measurements by Eckardt in a centrifugal impeller with no backswept

Later Krain [6] performed laser measurements on a backswept impeller, highlighting different behaviour from previous research; in particular he found a smooth pattern toward the rotor discharge section, while the wake flow arises inside the impeller channel. Great influence has been assigned to a swirling flow inside the rotor.

A valid explanation regarding some aspects of the jet-wake patterns is given by the secondary flow, which is typical of regions with non-uniform stagnation pressure and small shear-stress. The principal reason for secondary flow is the vorticity; in particular, the main contributions, as Johnson and Moore [7] noticed, are the curvature of the streamlines, R_n, and the angular velocity, ω, due to gradients of the stagnation pressure. These effects, combined with the curvature in the meridional plane and in the blade-to-blade surface, bring the movement of low stagnation pressure flow towards region of reduced static pressure. In order to take into account the influence of the curvature and rotation, a non-dimensional number has been spread, the Rossby number.

$$Ro = \frac{w}{\omega R_n}$$

Consequently, it is possible to assess that rotation is the dominant term in the hub-to-shroud surface. The most important curvature in a centrifugal impeller, with a low Ro and the wake fluid will be located on the suction surface; while if the Ro is high the low stagnation pressure area will be found in correspondence with the shroud wall. In [7], the authors conducted an experimental investigation on a radial impeller, explaining the development of the wake, its size and location and the influence of the secondary flow in the formation of the phenomenon. In a previous study, Eckardt [5] also focused on the secondary flow pattern in relation to the wake formation mechanism. He pointed out the strong connection between the secondary flow and the wake growth, because the former is responsible for movement of low-energy material fluid, as sketched in Fig. 11.

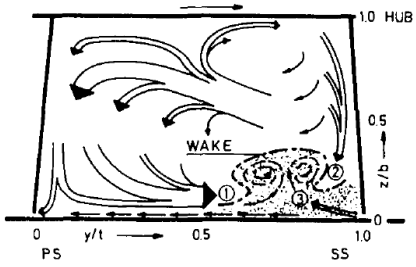

Fig. 11: Secondary flow pattern from Eckardt (1976)

As Cumpsty affirmed [8]:

The first signs of separation…were in the suction surface/shroud corner…The extent to which the separated region grows depends mainly on the ratio $\rho_1 A_1/\rho_2 A_2$ *of the machine, whilst the position of the wake is fixed by secondary flow considerations, primary the balance between the effect of the meridional curvature and the effect of rotation*

The highly non-uniform and distorted flow from the impeller discharge is a crucial point for diffuser design, since the primary purpose of this component is to recover the kinetic energy in the form of a rise in static pressure, minimizing the losses. Generally, in a vaneless diffuser the angular momentum remains constant and the tangential velocity component is usually larger than the radial component. In particular, the pressure rise comes mainly from

decelerating the tangential component by increasing the diffuser radius. Consequently, since the radial velocity decreases inversely proportional to the radius, the diffuser streamlines follow a logarithmic spiral, if the flow direction keeps constant. In addition, a more significant radial respect to tangential component generates a shorter path from the inlet to the outlet, this means reduced losses. A valuable influence, in this sense, is played by compressibility as well. Namely this increases the inclination of the mean flow towards the radial direction.

As observed by Dubitsky and Japiske in [9] inlet distortions have a great impact on vaneless diffuser flow behaviour, in particular a rotating distorted fluid leads to a work transfer between high and low velocity regions. This aspect has been highlighted also in [8]; effectively it is possible to distinguish two diverse phenomena: a reversible work exchange and irreversible mixing. However as Inoue stated [10], the energy transfer from the jet to the wake is negligible. On the other hand, from [9] it emerges the wall shear stress governs the flow behaviour in respect to the mixing shear stress between primary and secondary regions. It is worth noticing that significant impact of impeller-diffuser interaction is the impeller tip leakage flow, affecting blockage, slip and stage pressure ratio (PR), as stated in [11].

Generally, in most of the applications the vaneless diffuser is followed by a volute, a spiral-shaped channel of increasing cross-sectional area, whose aim is to deliver the discharged flow from the diffuser to the pipe system. An extra pressure increase can be accomplished in the volute. Part of the pressure recovery can be wasted with losses, especially at off-design operating condition. Hagelstein et al. [12] performed a very detailed investigation on the flow in a centrifugal compressor volute. From experimental results, they observed how the flow is affected by a strong vortex, with a very high swirl velocity gradient in the radial direction. While a secondary vortex produces an appreciable pressure difference from the centre to the walls of the volute. The authors underlined that the high velocity gradient is a source of loss. Moreover they observed a flow separation also in the volute, in particular a high kinetic energy flow region in the outer area of the volute and low pressure area, localized in the vortex centre.

In [13] Khalfallah and Ghenaiet confirmed the main flow features analysed above. They executed a transient simulation in order to study the rotor-stator interactions in a radial compressor. In particular these authors observed a clear jet-wake structure inside the impeller, while the scroll is dominated by a swirl flow. In correspondence with impeller shroud a recirculation flow area is formed and the high-velocity flow moves in the counter-direction of rotation. The high losses, due to high-velocity gradients, are concentrated around the tip exit impeller section. Instead, in the scroll a single vortex structure is recognized and it is characterized by high swirl, gradually reduced towards the outlet. The double function of the scroll at off-design operating conditions has been presented; at part-load the tongue is equated to a single vane, where the flow is split, partly back through the vaneless diffuser and the rest towards the scroll. At overflow the scroll acts as a nozzle, consequently the velocity increases and the flow impacts the tongue with a large incidence angle, leading to separation.

Multiphase fluid

During the experimental test campaign, the flow mechanisms described above have been observed under dry conditions. Significant similarities, especially related to the jet-wake structure, were detected also with the presence of a liquid phase. On the other hand, impeller-diffuser-volute interactions were very clear too. A detailed discussion about this subject will be dealt with in the following chapters.

The presence of a liquid phase has a significant effect on these phenomena, because of different velocities in the fluid: the water droplets have greater inertia than the gas phase. For this reason liquid particles cannot be dragged completely by gas.

Aerodynamic instability

Pampreen [14] defined stability as

The response of the compressor to a disturbance which perturbs compressor operation from a steady operating point.

Stability is strictly linked to whole system in which the compressor is integrated; certainly the working point is the intersection between these two different operating characteristics, as described in Fig. 12. So the system is considered stable if, during a perturbation, it returns to the original equilibrium point.

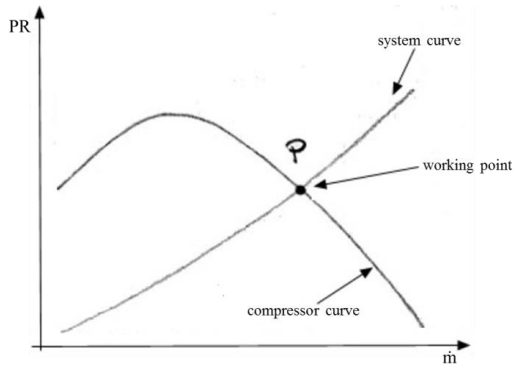

Fig. 12: Working point description

In [14], the author identifies two areas for stability: one related to operational stability, while the other is associated with aerodynamic stability. The former involves the complete compressor system and great influence is given by the slope of the machine characteristics. It is usual to connect a negative slope of the compressor characteristic to a stable operation. Although neither zero slope nor a positive one are absolute criteria to identify unsteady flow, it is recommended to set up an instability control point where the slope becomes zero. However aerodynamic stability is limited by unsteady state due to stall or surge.

Compressor instabilities

With regard to compressor aerodynamics, the main phenomena, cause of machine unsteadiness, are stall and surge. Day [15] used simple terms to affirm that stall is a flow disturbance along the tangential direction, while surge occurs in the axial one. Effectively the stall arises when the fluid separates from the surface of the blade (Fig. 13); in particular at low mass flow rate, the angle of attack might reach a critical value, causing the stall propagation towards other vanes, since the fluid separation, reducing the channel section, diverts part of the mass flow around it.

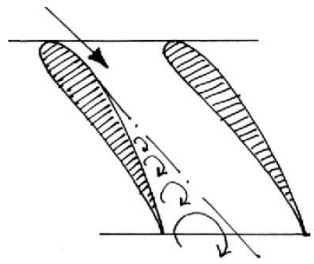

Fig. 13: Fluid separation during stall

Lennemann and Howard [16] disclosed the flow patterns during stall in a shrouded impeller, as sketched in Fig. 14. In these authors' opinion the phenomenon is strongly affected by secondary flow. The flow separation begins on the suction surface of the blade, blocking the channel exit and is reversed through the passage entry. Consequently fluid separates from the pressure side of the downstream channel, causing a relative eddy. This reverses its direction and forces the flow to move in the original unstalled direction.

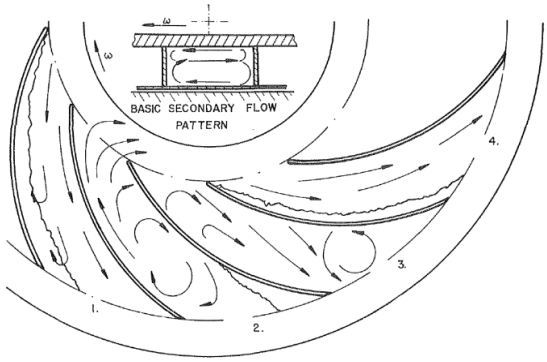

Fig. 14: Stall development in a shrouded impeller [16]

As Frigne and Van Den Bræmbussche [17] observed, the flow rate through the machine, is constant during a rotating stall. According to previous studies, they experienced rotating stall as a disturbance of the diffuser flow in a radial compressor as well as instability inside the impeller fluid. In particular they classified the instabilities into three diverse groups: diffuser rotating stall, abrupt impeller rotating stall and progressive impeller rotating stall. Each of these phenomena is generated by different flow interactions within the machine components. With particular regard to diffuser rotating stall, this is produced by interactions between the boundary layer and the inviscid core flow. In a previous study Jansen [18] postulated that rotating stall occurs when a three-dimensional flow separation comes up in the diffuser. He attributed the location of flow separation to the flow angle, inlet Reynolds number, Mach number and diffuser width. Later Senoo and Kinoshita [19], studied vaneless diffusers with different geometries and found that rotating stall is influenced by diffuser parameters; in particular for a large exit/inlet radius ratio and narrow width ratio the rotating stall occurs first and the diffuser stalls come later. The authors highlighted that the flow in a vaneless diffuser is not uniform across the depth, and near the walls an inward swirl flow may be produced. This effect could be the starting point of rotating instability.

More recently Sorokes et al. [20] observed a shift of the low momentum zone from the shroud to the hub side in a vaneless diffuser which is characterized by high flow rate and inlet impeller Mach number. This indicates that the phenomenon is a precursor to stall. They

suggested reducing the diffuser exit width in order to improve the working range and peak efficiency of the stage.

The phenomenon of surge is an unstable condition resulting in flow reversal and pressure fluctuations; it is characterized by low frequency oscillations, usually about 3-10 Hz [8]. This is the result of an excessive increase in the resistance of the system, so the compressor is not able to deliver continuous flow to the downstream collector, because of a pressure reduction. In Fig. 15 the effect of flow reversal approaching surge is reported; initially the backflow is close to the shroud and then the entire flow is reversed.

Cumpusty [8] identified two different types of surge that he classified as mild and deep surge. The mild process occurs when the operating point oscillates around the peak of the pressure rise-mass flow curve, while if the instability is violent and results in a reverse flow from the suction, deep surge develops.

Toyama et al. [21] performed a detailed study on surge in centrifugal compressors. Fig. 16 reports pressure variation during surge at 85% speed. It is evident that there is low frequency variation in the pressure before surge in the diffuser throat. It is interesting to note the sudden pressure rise just before backflow. The authors affirmed this effect is due to a boundary layer change.

In [19], discussing about the critical condition of surge, and focusing on a backswept impeller, it emerges its characteristic curve has a large negative gradient. So combining the characteristics of the compressor and a vaneless diffuser, the gradient is still negative despite the pressure loss in the diffuser component, which is attributed to the wall friction and exit dissipations of kinetic energy. The authors stated that a system does not experience surge if a sort of stabilizing effect is present and neither the impeller nor the diffuser stall.

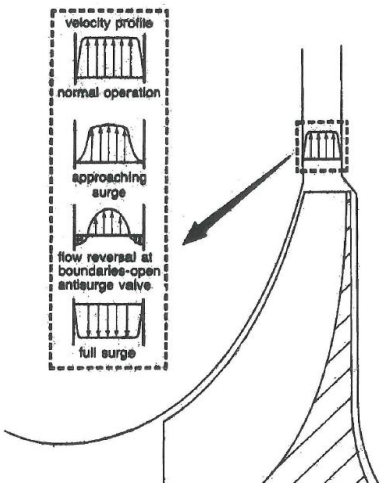

Fig. 15: Flow reversal when approaching surge.

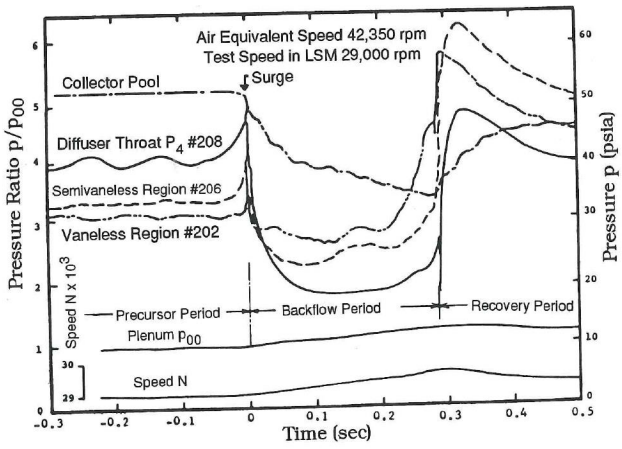

Fig. 16: Pressure variation during surge, from [21]

Multiphase fluid

The spectrum analysis revealed a powerful means for studying the aerodynamic instabilities with the presence of a liquid phase during transient flow. Basically the fast Fourier transformation converts time dependent data into the amplitude/frequency range, by decomposing a time-varying signal into pure tones. Usually these components are sinusoidal wave forms of constant frequency and amplitude.

By Fourier analysis a variable, expressed as a function of time and acquired over a period of time with a constant sampling rate, is transformed into a series of oscillatory functions. Each of these functions has a characteristic frequency that reflects the amplitude of the oscillatory function at the corresponding frequency.

The dynamic pressure transducers, employed during the left limit investigation, are used to obtain a spectrum where the blade passing frequency and subsynchronous frequency are monitored.

This technique is applied by several researches; Gonzàlez Diez et al. [22] used dynamic simulations to propose and validate a numerical model based on a modified Greitzer's model in order to reproduce the behaviour of a centrifugal compressor. Kang and Kang [23] examined a high-speed centrifugal compressor with the aim of identifying the stall precursor condition and developed a reliable stall warning method. Sampled data have been analysed by spatial Fourier transform and compared with the travelling wave energy technique. With the same intent, Liu and Zheng [24] collected various dynamic data from a high-speed centrifugal compressor and demonstrated that the standard deviation of signals provides a feasible index for surge detection. Bianchini et al. [25] produced a broad guideline to characterize the rotating stall with dynamic pressure sensors in a vaneless diffuser. During rotating stall, the distribution of pressure fluctuations is marked by a component higher than the blade passing frequency (BPF). Usually, the vaneless diffuser rotating stall is displayed as a pressure fluctuation at a subsynchronous frequency in a range between 10 and 40% of the revolution frequency (f_{1XREV}). Aretakis et al. [26] and later Morini et al. [27] verified the chance of catching unstable operating conditions using acoustic and vibration measurements.

Some considerations concerning performance and unstable operating conditions in the presence of water emerge from experimental work by Day et al.[28], analysed the effects of water ingestion on the performance of an axial flow compressor. Here, premature stalling was observed in most cases. Roumeliotis and Mathioudakis [29] found the whole compressor stall limit and stall margin were negatively influenced by water injection. In particular, a reduction

on the surge line with respect to mass flow was detected. Different results and conclusions were obtained from a system stability analysis in wet conditions carried out by Minghong and Qun [30] and [31]. Wet compression has stabilizing effects on both rotating stall and surge. Comparable deductions derive from an investigation of a single stage centrifugal compressor exposed to wet conditions [32]. Grüner reported a delayed onset of instability because of the presence of the liquid.

Wet gas compression: a general overview

This section describes the main outcomes with two-phase flow. Attention is principally paid to the flow regime and mechanisms prevailing under wet operating conditions. A discussion about the impact of liquid on machine behaviour and working conditions both overload and part-load is offered.

A limited number of research works on wet gas compression has been already published, since this is a relatively new area of study. A general trend has been identified; the fluid is characterized by a small amount of liquid up to 5% on volume basis, so the flow is even more complicated, compared to dry gas flow. The pattern is annular: a thin liquid film is formed on the channel walls and a dense droplets flow describes the core. This results in a thermodynamic and kinematic no equilibrium and because of momentum, heat and mass transfer between the phases strong losses arise. The effects due to density changes, phase interactions and compressibility variations make the standard calculations inadequate, so new methods to estimate performance are fundamental. On the other hand, knowledge of the operational range, the flow regime and evolution is crucial in designing a new efficient wet tolerant apparatus. The present work should be included in this context.

In [2], the authors present the trends observed during wet gas compression tests. In general a significant power consumption increase and a pressure ratio increment are registered. In addition, the temperature ratio decreases and the liquid droplet size has no effect if injected far enough upstream of the compressor to allow a natural two-phase flow regime to develop.

Concerning the wet gas impact on compressors, Hundseid in [33] explained all the multiphase effects. The changes in fluid density are most relevant; in particular the pressure ratio will increase with increasing the fluid density. The evaporative cooling contributes to a drop in discharge temperature. The principal influences are observed for the speed of sound and the Reynolds number. In the first case, increasing the liquid content, the speed of sound, which affects the Mach number, decreases. On the other hand, a liquid film formation on the surface varies the roughness and, consequently, the Reynolds number. Frictional losses, blockage and disturbances are associated consequences.

In [34], the authors mainly performed a thermodynamic analysis of a single-stage centrifugal compressor. They observed a pressure ratio increase by decreasing the gas mass fraction. The presence of liquid caused a reduction in the temperature ratio, as well as power consumption. Some partially different results came from [35] and [36], but they confirmed a rise in absorbed power, owing to large internal flow losses. The analyses in [35] – [37] found that aerodynamic performance of the compressor was significantly affected by liquid injection. In particular, an increase in terms of pressure ratio has been shown with respect to dry-gas performance. This effect probably reflects higher fluid density. A reduction in compressor specific work and discharge temperature has also been highlighted.

A reduction of compressor efficiency that increases the mass fraction of liquid because of larger power absorption is reported in [33]. Concerning aerodynamic instability

investigation under wet gas conditions, Grüner et al. [37] analysed the compressor behaviour. They propose that liquid injection delays instability inception. Brenne [38] described pressure recovery in a straight-walled diffuser with single-phase airflow and two-phase mixture. His work focused on the measurement of pressure recovery and visualization of two-phase flow in a straight-walled diffuser.

Hundseid et al. [39] clarified that the standard parameters based on dry gas theory are not applicable for estimating wet performance, especially because of sensitivity to temperature variation. So they proposed a corrected formula to calculate the polytropic head and efficiency, employing Wood's model.

Conclusion

This chapter summarizes the parameters for performance analysis with the presence of a liquid phase. Rudiments about velocity triangles at different operating conditions, e.g. design and off-design points, are supplied. Connections with stability and range are given.

The complex nature of multiphase flow requires a review of literature concerning the flow pattern inside a centrifugal compressor. In dry gas the jet-wake patterns are highlighted and interactions between machine components are emphasized. This chapter supports the thesis objective about the visualization of flow mechanisms inside the impeller and diffuser and the documentation of the flow path.

In addition an overview about unstable phenomena in centrifugal compressors and a valid procedure to execute left limit investigation under wet conditions is reported. The fast Fourier transform analysis, monitoring the blade passing frequency, results a valid anti-surge method. This represents the theoretical basis to reach the thesis objective about the machine working range and the effect of the liquid presence on stall and surge.

3. Test rig

An advanced test facility has been developed to identify the fundamental mechanisms related to wet compression and understand the behaviour and capability of a total subsea compression system [40].

Description

The rig (Fig. 17) is a single-stage centrifugal compressor, comprising an impeller, a vaneless diffuser and a variable section discharge scroll. For the compressor cross-section refer to Fig. 1

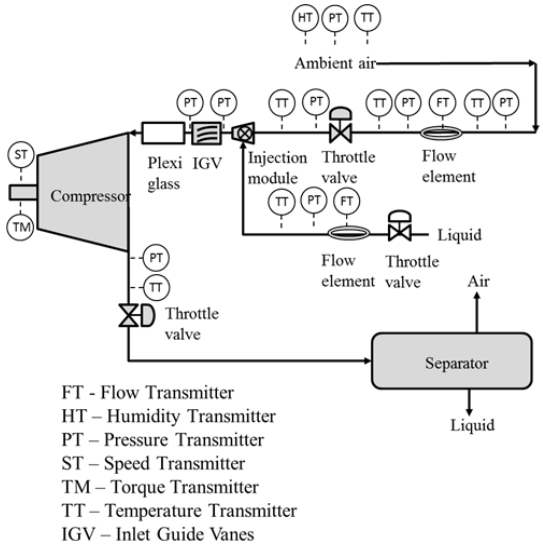

Fig. 17: Piping and instrumentation diagram of the test rig

The working fluid is an air-water mixture. Grüner and Bakken [37] have compared water performance data from the rig with corresponding results from a high-pressure hydrocarbon compressor test. This evaluation showed that testing with water at low pressures gives the same performance trends as high-pressure hydrocarbon tests. Previous experience has shown that a comparison of performance between different fluids and inlet conditions must be based on the corresponding GMF.

The main characteristics of this open-loop rig are the observation slots with Plexiglas (Fig. 18) for the multiphase flow at the impeller inlet and discharge, frontal diffuser and volute section. Visualization of the fluid flow path is vital to understand the performance under different flow regimes and liquid content. The inspection windows simplify the flow analysis, since the entire path of fluid is visible from the axial entry on the impeller tip to the volute, through the impeller discharge section and the diffuser.

Fig. 18: Plexiglas windows for flow visualization

Multiphase flow measurements inside the compressor channels have proved difficult, and visual observation accordingly plays an important part in understanding wet compression performance. Considerable attention has been paid to increasing visual access to the flow path through the compressor. With the current windows the outlet pressure is restricted to 1.5 bar. In addition the frontal diffuser is equipped with different instrumentation in the radial direction, as shown in Fig. 19.

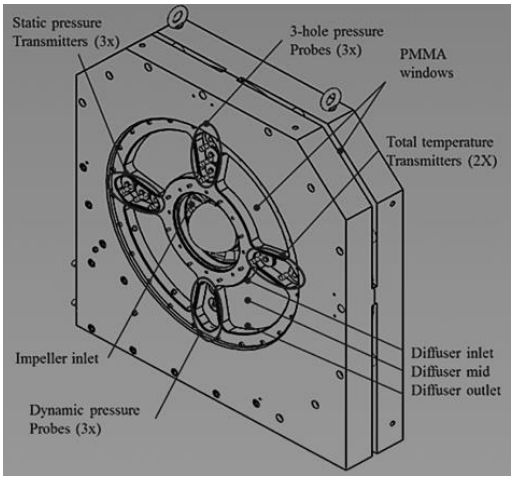

Fig. 19: Frontal diffuser section and instrumentation detail

Fast-acting, high-precision air inlet and discharge valves and a water injection valve make it possible to test transient flow regimes, by throttling the flow. The high-speed electric motor and the related advanced drive complete the compression system and permit a maximum continuous speed equal to 11000 rpm.

The ambient air flows through an inlet pipe; while the water is injected upstream the impeller inlet through a water injection module consisting of 16 nozzles equally distributed around the pipe wall (Fig. 20). Water flow is controlled by regulating supply pressure and the number of active nozzles and is measured by an electromagnetic flowmeter. The mass flow of air is measured using an orifice plate.

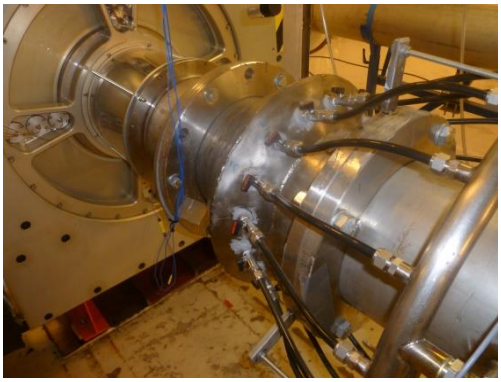

Fig. 20: Water injection system

The impeller is fixed to the shaft of a bearing pedestal, which is used to prevent water penetrating the electric motor. The bearing pedestal and electric motor are connected through a torque meter, permitting accurate measurement of static and dynamic compressor power. Table 1 presents the main compressor data for the new section. The characteristic ranges are indicated for some impeller values, because the actual design cannot be disclosed.

Impeller outlet diameter (D_2)	400mm
Impeller width (b_2)	10-45mm
Impeller blade angle (β_2)	45-55º
Diffuser width (b_3)	20mm
Diffuser ratio (D_3/D_2)	1.7
Inlet hub diameter	250mm
Outlet pipe diameter	200mm

Table 1: Main compressor dimensions

The axial design of the scroll is symmetrical. Two tanks at the outlet separate the wet gas outlet flow. The test rig operating range and conditions are presented in Table 2

Suction conditions	Atmospheric
Test fluids	Air/water
Air-flow range	0-3 kg/s
Water-flow range	0-5 kg/s
GVF range	99.93-100%
GMF range	40-100%

Table 2**:** Test rig operational range

The acquisition system for the test rig measurements is a PC-based platform, which permits synchronous sampling up to 20 kHz. Performance testing is in accordance with ASME PTC-10. Table 3 presents measurements acquired during testing with relative accuracy.

Instrument section	*Accuracy*	*Unit*
Ambient temperature	± 0.2	ºC
Ambient pressure	± 0.15	hPa
Relative humidity	± 1	%
Temperature flow element	± 0.15	ºC
Pressure diff. flow element	± 0.04	%
Dynamic pressure diffuser	0.14	mbar
Static pressure diffuser	± 0.002	bar
Total temperature diffuser	± 0.009	ºC
Three hole probe diffuser	0.11	%
Inlet pressure compressor	± 0.3	%
Inlet temperature compressor	> ± 0.1	ºC
Outlet pressure compressor	± 0.3	%
Outlet temperature compressor	> ± 0.1	ºC
Water flow meter	± 0.5	%
Shaft speed	± 5	rpm
Shaft torque	± 0.48	%

Table 3: Test rig instrumentation

Conclusion

An advanced open-loop test facility was validated under multiphase conditions. Special inspection windows were installed on the frontal diffuser and inlet pipe sections. In addition, the rig was equipped with fitting instrumentation, in order to execute the experimental campaigns.

4. Test campaigns and results

This chapter gives an overview and description of the different test campaigns, on which the experimental work has been based. The experimental work is the main contribution from the author, who planned and carried out all the tests. The performed campaigns are:

- Performance test;
- Flow visualization analysis;
- Left limit investigation;
- Erosion test.

Text matrix

Performance test

In order to create a baseline under dry and multiphase working conditions, performance tests were carried out. The first insight concerning the impact of liquid on pressure ratio, efficiency, power consumption and work coefficient is taken.

In Tab. **4**, the selected speedlines for performance tests are presented. Three diverse rotational speeds are chosen: 6000, 9000 and 11000 rpm; for each characteristic different values of gas mass fraction have been tested, from totally dry (GMF equal to 100%) to 70% of GMF. In general, for each curve, six points have been tested. All the test points had to satisfy strict criteria to reach steady state, as in Table 5. In particular, the values were acquired by averaging each parameter for 60 s, when the band and slope criteria were satisfied over a period of 10 minutes.

Speed [rpm]	**Gas Mass Fraction [-]**				
6000	100%	95%	90%	80%	70%
9000	100%	95%	90%	80%	70%
11000	100%	95%	90%	80%	70%

Tab. 4: Selected conditions during performance test

	Time Window [s]	**Max Band [%]**	**Max Band [u.m.]**	**Max Slope [u.m./s]**
$\varphi_{WET\ in}$	600	±2.5%	0.001	1.6667E-06
Mu_dry	600	±1.0%	0.004	6.6667E-06
FtF_PR_static	600	±1.0%	0.011	1.8333E-05
FtF_ΔT	600	-	±0.05°C	8.3333E-05
FtF_ΔT (wet tests)	600	-	±0.12°C	0.00015
Torque	600	±0.8%	±0.2 Nm	0.00033333
GMF	600	±0.5%	0.005	8.3333E-06

Table 5: Stability test criteria

Visualization test

After the performance test, the flow visualization has been studied. This campaign has been split in two different stages: the flow regime in correspondence with the impeller eye and diffuser section was analysed, then a more detailed investigation with fluorescent injection has been executed. The test conditions for flow visualization are given in Table 6.

The values represent the right balance for testing with a moderate amount of water so as to have a clear view of the section.

Speed [-]	Gas Mass Fraction [-]			
6000	92%	-	90%	-
9000	-	95%	90%	80%

Table 6: Test conditions for flow visualization

Injection of fluorescent liquid, highlighted by an UV lamp, has been executed in correspondence with impeller labyrinth seal, in order to clarify the effect of liquid leakage from a seal on the reverse flow formation at the impeller tip area, and within the diffuser section. In particular injection points were located in correspondence with the diffuser inlet and outlet, as sketched in Fig. 21. In this case different positions in the axial direction have been identified, moving from the shroud to the hub side across the diffuser width. The main goals were to visualize the streamline and flow trajectory and identify the influence of the liquid phase presence.

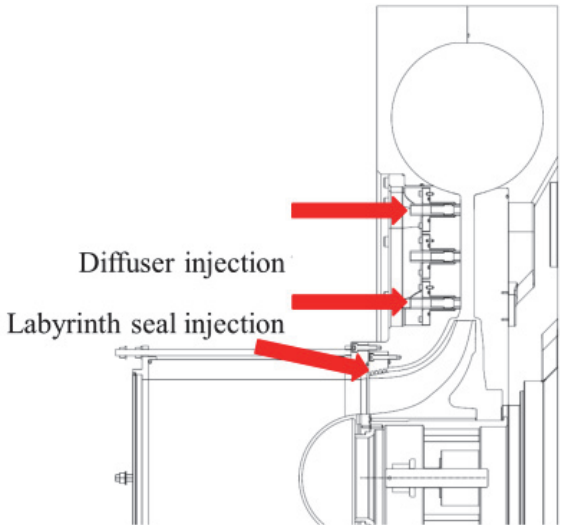

Fig. 21: Cross section showing the fluorescent injection point

Left limit investigation

In addition, a left limit investigation has been performed to study the machine operating range with the presence of the liquid. Signals from high-response dynamic pressure transmitters have been post-processed through fast Fourier transform to detect unsteady phenomena. The sensors were installed flush-mounted in three different radial positions: the diffuser inlet, the middle and the outlet section, as given in Fig. 22. The dynamic pressure sensors are furnished with PCB Piezotronics and have a resolution of 0.14 mbar.

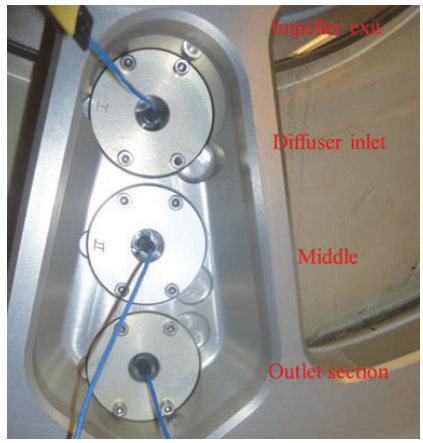

Fig. 22: Radial position of high-response transmitters

Erosion test

In order to identify areas more exposed to erosion and roughly estimate the erosion rate, a qualitative erosion test has been performed. For this purpose the impeller has been painted manually with an airbrush, with three layers of soft painting (Fig. 23).

Fig. 23: Impeller painting

The erosion tests were carried out following the schedule reported in Table 7. The impeller has been subjected to run with the presence of liquid during longer and longer time periods; moreover periodic visual inspections have been programmed.

Time [hours]		Action
From	to	
0	0.5	Run in wet conditions
0.5	1	Optic/Boroscope inspection
1	1.5	Run in wet conditions
1.5	2	Optic/Boroscope inspection
2	3	Run in wet conditions
3	3.5	Optic/Boroscope inspection
3.5	5.5	Run in wet conditions
5.5	6	Optic/Boroscope inspection
6	8	Run in wet conditions

Table 7: Erosion test

The thermodynamic conditions selected for the erosion test are reported in Table 8. It should be noted the working conditions are very strict, since the impeller was supposed to work at heavy regime.

Speed [rpm]	**Mu**	**φ**	**Q_g [m^3/s]**	**GMF**	**$\dot{m}_l$ [kg/s]**
11000	0.656	0.062	1.80	50%	2.14

Table 8: Thermodynamic conditions during the erosion test

Results

This section provides the results from all the test campaigns. In order to simplify matters, the results have been divided in four different sections, related to each experimental field of research.

Performance test

The reported results apply only to operating speeds of 11000 rpm, since, modifying the rotational speed, no significant variation has been detected. The actual parameters have been normalized by a corresponding measured value at the design point.

In Fig. 24 the flange to flange pressure ratio is plotted. It can be seen that when decreasing the gas mass fraction, the stage PR drops. In particular, in correspondence with the high flow rate, a reduction of stage performance is more evident at lower GMF due to larger losses. With 95% gas mass fraction, the water presence does not significantly affect the pressure ratio with respect to dry conditions. These results contrast with previous industry test experience, e.g. [36], since in this case the impeller is characterized in a condition with a higher density ratio. However, other results such as a reduction in the operating range and a curve slope change are confirmed by the present test, especially for tests with a large liquid content.

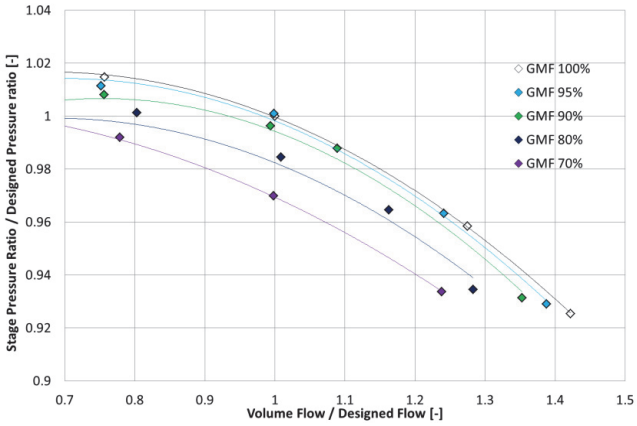

Fig. 24: Non-dimensional stage pressure ratio, at 11000 rpm and different values of GMF

Under wet conditions the polytropic efficiency decreases by increasing the content of liquid in the flow rate, as shown in Fig. 25. This effect is caused by higher power consumption, because of a greater amount of mass flow. The deterioration mechanism of performance under wet conditions is clearly evident: the lower the GMF, the higher the efficiency drop. From total dry to 95% of the gas mass fraction, 12% losses in polytropic efficiency are detected at the best efficiency point. While from total dry to 70% GMF a reduction of about 45% is observed.

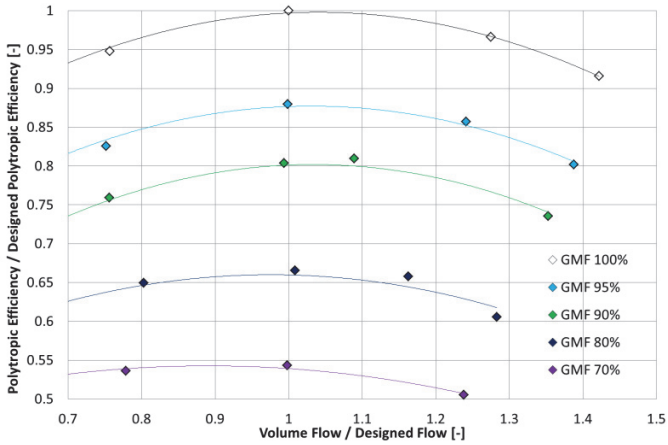

Fig. 25: Non-dimensional stage polytropic efficiency, at 11000 rpm and different values of GMF

The trend of work coefficient as a function of the gas mass fraction is presented in Fig. 26. τ rises monotonously when decreasing the GMF because of increased mechanical work caused by greater power consumption, as stated above. The impeller peripheral velocity may also affect the value. As liquid has higher inertia than the gas phase a reduction in mixture velocity could balance augmentation in the mass flow rate. The same trend of τ has been obtained during tests at 9000 rpm. For the gas mass fraction equal to 95% - 90%, the work coefficient increment is uniform and no variation of slope is observed, while for lower GMFs a deviation of slope is also highlighted.

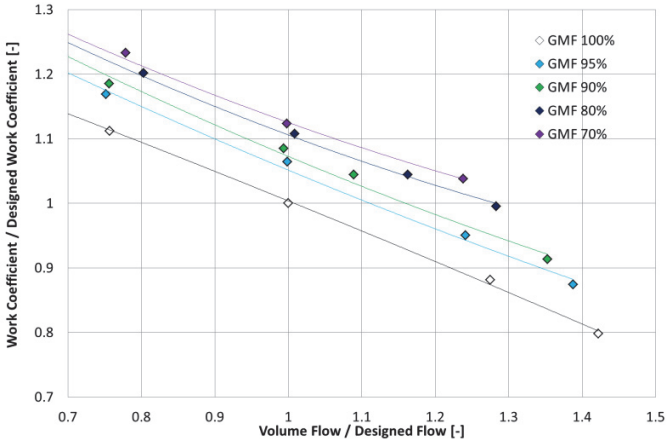

Fig. 26: Non-dimensional stage work coefficient, at 11000 rpm and different values of GMF

In Fig. 27 absorbed power is plotted against non-dimensional volume flow. It is clear that increasing the amount of liquid the power consumption grows. It should be noted that the mechanical power is proportional to the work coefficient; consequently the power will increase because of the rise in this term too.

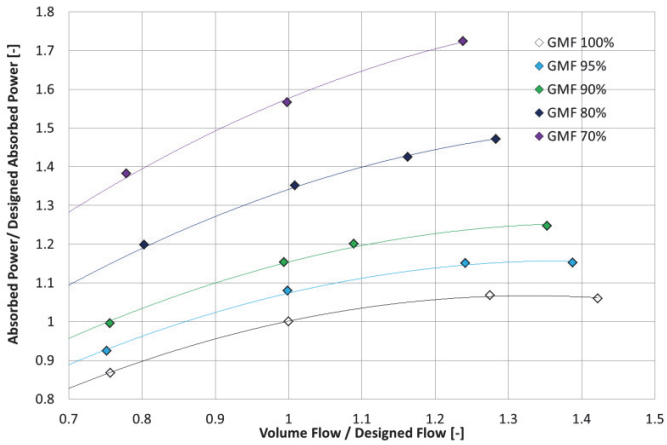

Fig. 27: Non-dimensional stage absorbed power, at 11000 rpm and different values of GMF

It is evident that the water injection has the direct effect on reducing the performance of the centrifugal compressor: increasing the liquid amount, the PR and efficiency reduce accordingly. The trend is confirmed by the power consumption trend too. It should be noted that the design of the machine is not optimized to handle multiphase flow.

Flow visualization

This section provides results regarding the flow visualization campaign. In order to simplify the reading, the results have been divided in two sections: one related to the impeller and the other to the diffuser and volute.

Impeller

The flow visualization with the presence of a liquid phase is vital for the optimization of rotating machinery design. Several test campaigns were performed in order to clarify the behaviour of each component. For this purpose an experimental operation has been executed focused on the impeller inlet section in order to investigate the progression of instability.

Fig. 28 displays the evolution of the impeller inlet flow pattern approaching surge (reduced flow coefficient). The reported results apply only to operating conditions of 6000 rpm and a GMF of 0.92, because the smaller amount of water allows a clearer visualization of the liquid accumulation. However, the same characteristics are observed during different operating conditions.

When reducing the flow coefficient, a gradual rise in the liquid boundary layer has been registered upstream from the impeller inlet tip region. Moreover, the accumulated liquid forms “waves” that move in both tangential and axial directions to create a swirling motion, indicating a fluctuating phenomenon. The accumulated liquid is maintained by the reverse airflow at the impeller inlet tip, blocking the inlet annulus section.

Fig. 28a presents the initial liquid accumulation at the annulus boundary layer. When the flow coefficient is reduced, Fig. 28b, it should be noted that the turbulence of the liquid phase develops in a tangential direction because resistance is lower there. An increase in turbulent motion and swirls is detected at φ 0.0236 (see Fig. 28c). Forces from backflow overcome the opposition of the incoming flow, and the boundary layer consequently also moves in an axial direction, as reported in Fig. 28d. Fig. 28d and Fig. 28e show an accumulation of water in the bottom of the inlet pipe; which corresponds to a complete formation of water film all around the pipe.

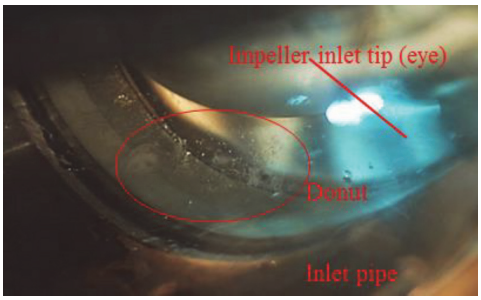

(a)

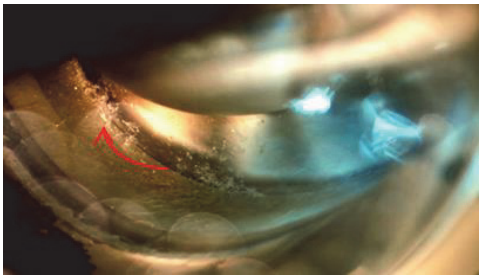

(b)

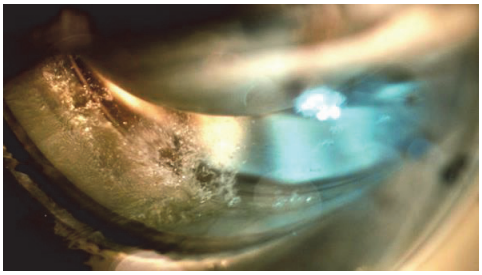

(c)

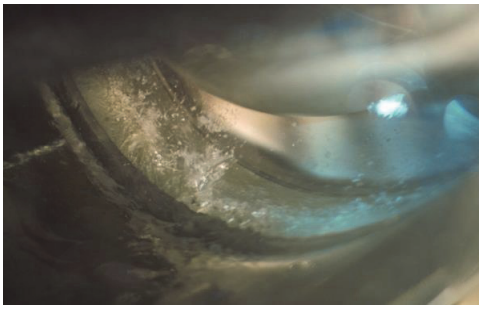

(d)

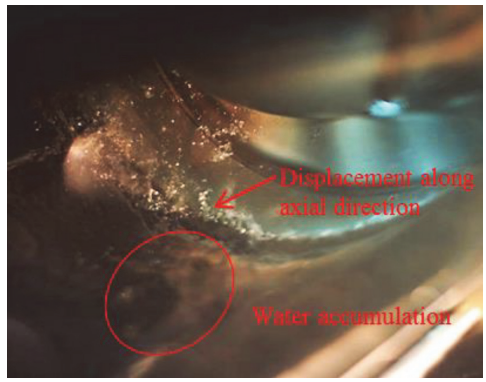

(e)

Fig. 28: Characteristics of flow development during surge, at 6000 rpm, 92% GMF and φ of a) 0.0305, b) 0.0286, c) 0.0263, d) 0.0235 and e) 0.0203

Accumulating water gradually forms a "doughnut" (Fig. 29) and a transient flow pattern in both axial and tangential directions. In addition, a boundary layer shift along the axial direction is observed.

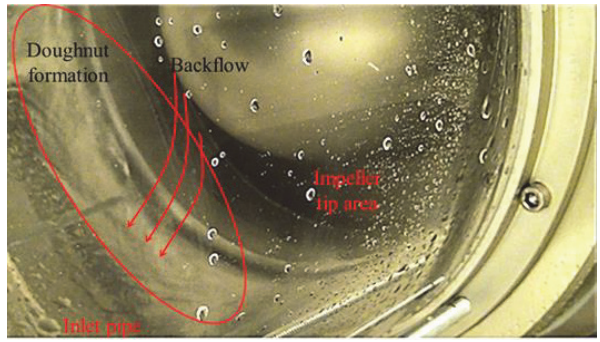

Fig. 29: Backflow with doughnut formation at 6000 rpm and 90% GMF

In order to explain the effect of the reverse flow that occurs at the impeller inlet, the gap between the impeller shroud and the frontal diffuser was studied more closely. Leakage of liquid from the labyrinth seal towards the compressor inlet section may significantly influence the impeller inlet regime and grows with the pressure rise, approaching surge. The effect of this leak on the documented "doughnut" formation has been investigated by fluorescent liquid injection, highlighted by a UV lamp, directly into the labyrinth seal.

Fig. 30 presents the results obtained at 9000 rpm and 90% GMF. A smaller part of the injected fluorescent appears at the impeller tip area, in particular observing the flow regime and decreasing the flow coefficient: it is clear that leakage from the labyrinth seal increases when diminishing the mass flow rate. The red ovals mark the reverse fluorescent from the labyrinth seal.

It should be noted that the tested operating conditions are not characterized by any backflow event and accumulation of liquid on inlet pipe; so the unstable phenomenon at the impeller inlet, individualized by doughnut formation, is partly caused by leakage of liquid from the labyrinth seal. Part of the sucked liquid, during wet operation, escapes from the gap between the impeller and diffuser components.

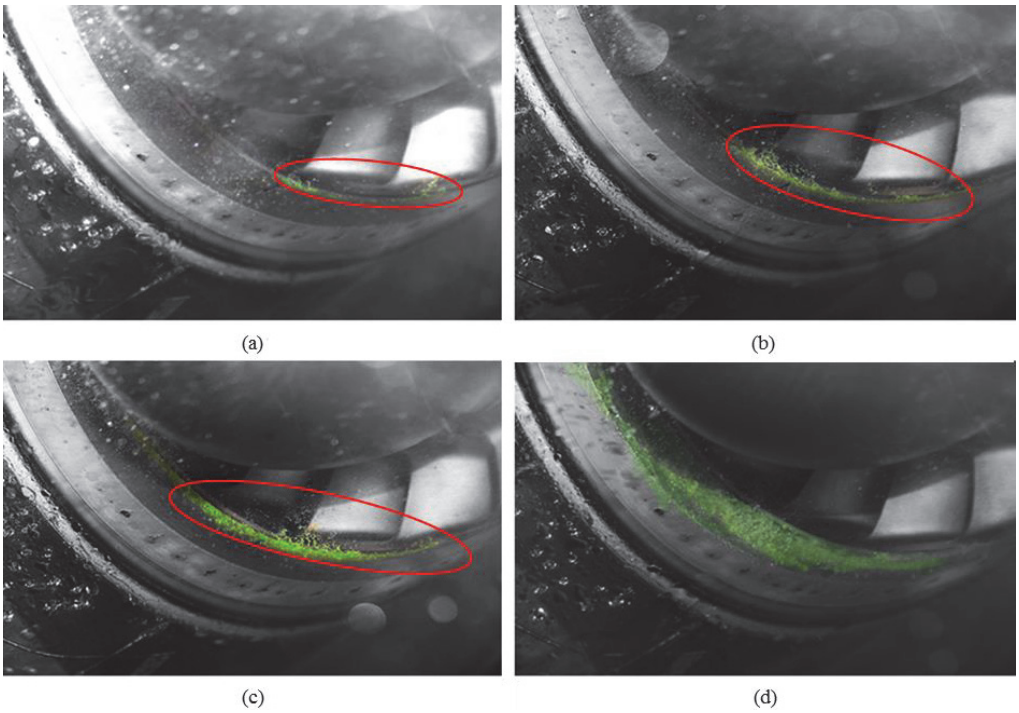

Fig. 30: Labyrinth seal injection, 9000 rpm GMF 90%; (a) φ 0.035, (b) φ 0.03, (c) φ 0.0285, (d) φ 0.025

Diffuser and volute

The campaign performed on the diffuser was split in two main steps: flow path visualization by a digital single-lens reflex camera; particular attention was paid to settings and the highest shutter-time (1/8000 s) was selected for "freezing" the path. After, focus was on streamlines and flow trajectories, marked by fluorescent liquid injection, refer to Fig. 21.

Fig. 31 displays the flow path at the design point (φ = 0.065) under multiphase conditions, with 90% GMF. In Fig. 31a, two different diffuser flow regimes are distinguished. Two zones are revealed: a mixing and a film region. The former appears to correspond with the diffuser inlet section and is characterized by small waves which is an indication of diverse velocities between the two phases. The gas flow, with an increased speed, drags the water towards the main flow direction. The latter, marked by a rectangle, is localized on the mid-diffuser section in a thin film region. This zone is situated on the shroud side, on the left corner and is characterized by a higher gas mass fraction with respect to the surrounding flow. An indication of the main flow direction is obtained as well.

Utilizing stroboscope light, Fig. 31b exposes high GMF jets coming out from the impeller vanes. The visualization documents the relative flow field velocity and segregation. The jet patterns are located on the impeller shroud-suction side.

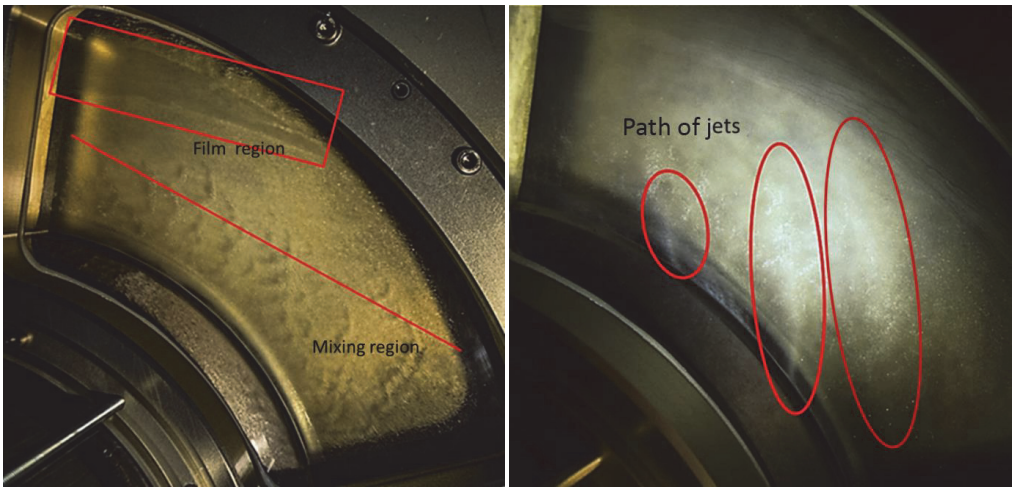

(a) (b)

Fig. 31: Design point, φ = 0.065, at 9000 rpm with 90% of GMF; (a) flow path, (b) path of jet-wake

At a higher flow coefficient than 0.065, Fig. 32, the jets appear clearly with similar inclination to the ones in Fig. 31b, which presents a clear radial orientation. It is worth noting that the jet inclination is opposite to the rotating direction of the impeller. However they become less intense and more dispersed by decreasing the flow coefficient, as given in Fig. 33, because of the rate reduction and the consequent decrease in the absolute velocity angle. Diminishing the flow coefficient, the shift in the diffuser flow regime is clearly visualized, as well as the occurrence of an unstable region, where a highly unsteady flow prevails.

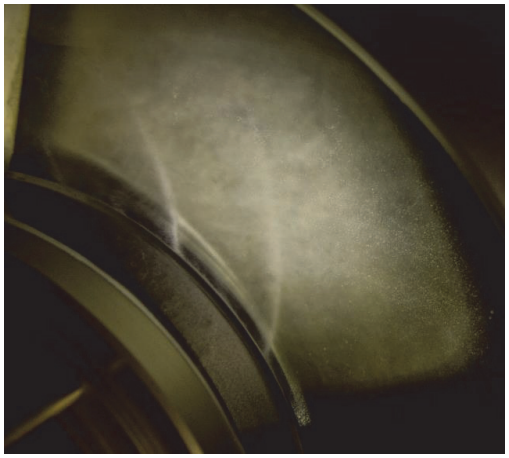

Fig. 32: Jet-wake at open valve, 9000 rpm with 90% of GMF

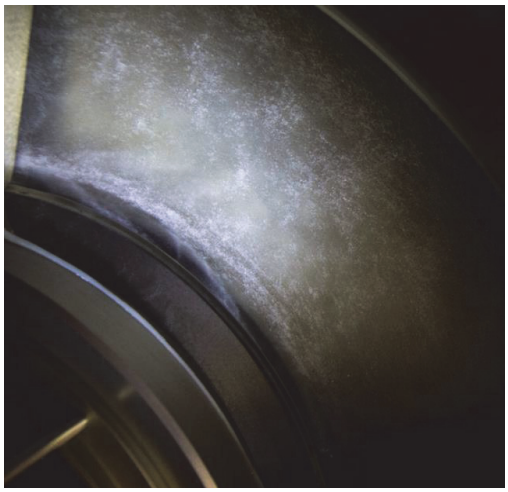

Fig. 33: Jet-wake for φ = 0.03, at 9000 rpm with 90% of GMF

Jet patterns are visualized in Fig. 34. They are caught at design point, with 9000 rpm of speed and 80% of GMF. The flow path is the same observed at 90% of gas mass fraction, but an evident curve in the tangential direction is shown in the window on the left hand side. This structure is a clear indication of the mainstream path under wet conditions.

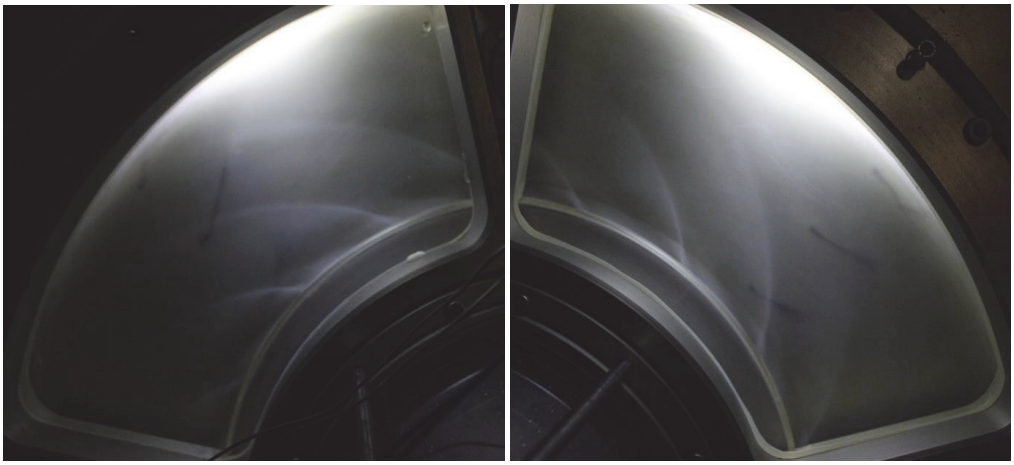

Fig. 34: Jet-wake at design point (φ = 0.065), 9000 rpm and 80% GMF

In Fig. 35 (a) – (c) flow regimes under unstable conditions, characterized by flow coefficients lower than 0.03, are presented for 9000 rpm at different values of GMF, 95%, 90% and 80% respectively. Different flow paths are individualized at these operating conditions.

In Fig. 35a, diverse flow behaviour is observed compared to design conditions (Fig. 31a). In particular in the diffuser discharge section, a distinct region marked by high GMF appears; this develops along the tangential direction. Turbulent motion is predominant, which might be caused by reverse flow from the volute. In the centre, a thin layer is visible, as above in Fig. 31a. While at diffuser inlet section, an accumulation of liquid phase is recognized by more distinct “white colour”. This phenomenon reflects flow fluctuations occurring in the

impeller inlet section, as observed in previous paragraph. In [38] a similar zone has been distinguished in correspondence to the wall diffuser, and it was assimilated by the author to a channel blockage.

Fig. 35b presents undisturbed and uniform flow, marked by stripes, in the diffuser mid-section; a similar path has already been identified by Brenne [38]. It is still possible to identify a thin region of turbulent flow in correspondence with the diffuser inlet and outlet section.

Large ripples are observed at 80% of GMF, in Fig. 35c. This mixing region prevails completely in the diffuser section, presenting similarity with Fig. 10. Brenne also detected a continuous wave region in his work [38]. In correspondence with the diffuser inlet, as already seen with 95% of GMF, an accumulation of liquid phase is identified. A tangential flow direction is predominant at this working condition as shown by the waves, and a back flow through the impeller should be taken into account.

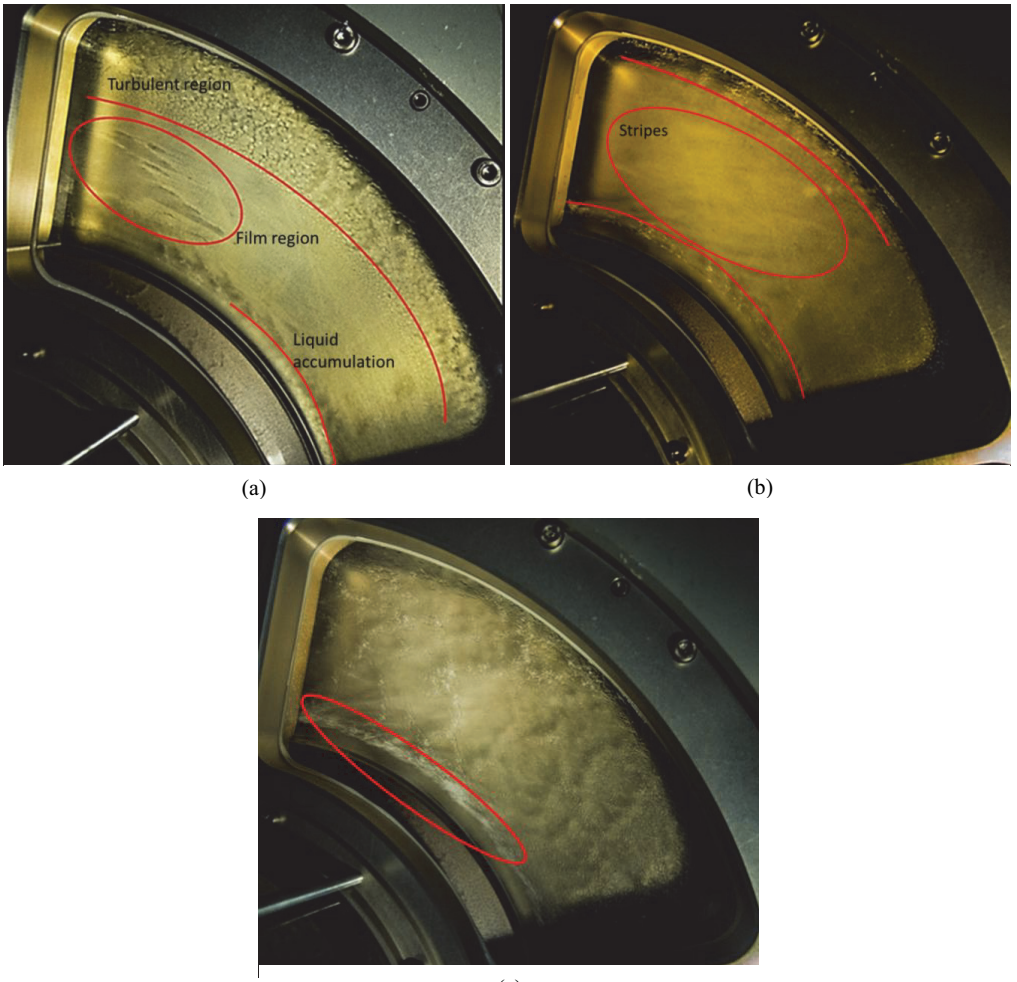

(a) (b)

(c)

Fig. 35: (a) $\varphi < 0.03$, at 9000 rpm with 95% of GMF; (b) $\varphi < 0.03$, at 9000 rpm with 90% of GMF; (c) $\varphi < 0.03$, at 9000 rpm with 80% of GMF

In Fig. 36, flow regime at 6000 rpm with 90% GMF is presented. The separation between turbulent and steady flow is evident.

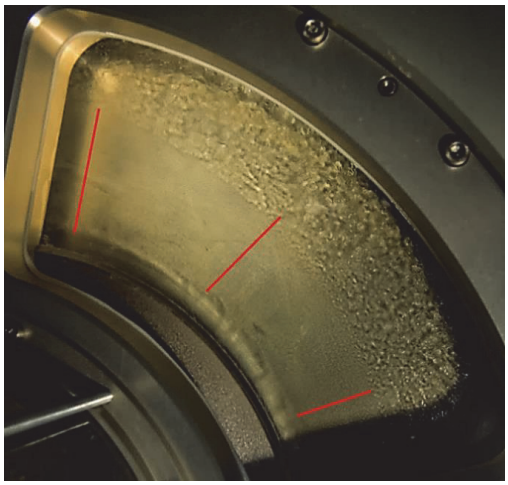

Fig. 36: $\varphi < 0.03$, at 6000 rpm with 90% of GMF

The regime registered at 9000 rpm and 95% GMF (Fig. 35a) is similar to the flow path at 6000 rpm and 90% of gas mass fraction (Fig. 36): two distinct regions can obviously be recognized. A separation between the gas-liquid mix and the air area is evident. Moreover, on the diffuser discharge area a turbulent region is visualized. This is larger at 6000 rpm than 9000 rpm and indicates backflow from the volute, as already documented.

The behaviour detected in Fig. 35a deviates from 6000 rpm due to the presence of a thin film in the middle, already noted at the design point (Fig. 31a).

The turbulent region around the diffuser outlet section narrows at GMF 90%, as in Fig. 35b. While, at 80% of GMF (Fig. 35c), ripples fill the entire diffuser section, since a mist flow, characterized by a moisture increase, prevails.

Fluorescent injections have been carried out in correspondence with the diffuser inlet and outlet. Fig. 37 to Fig. 39 present the results at the diffuser inlet section at 9000 rpm and 90% GMF, while Fig. 40 shows the effects relating to diffuser discharge injection under the same working conditions. In the former case, the reported results are relating to the hub and shroud sides, while for the diffuser outlet only the shroud side is exposed.

In Fig. 37 the flow path at a corresponding flow coefficient of 0.065 is visualized. Two trajectories are clearly evident on the hub side of the diffuser inlet (Fig. 37a). In particular, one is nearly radial, whereas the second one has a more spiral path: the streamline forms a logarithmic spiral, typical of a vaneless diffuser. In this case, the radial pattern is associated with the presence of a secondary flow, which is produced when the main flow has a non-uniform stagnation pressure. This effect is assigned to discontinuous impeller discharge velocity. However, a different explanation can be offered which is due to the presence of a liquid phase, characterized by a higher density compared to gas. Thus greater inertia in the liquid neutralizes the deceleration effect of the diffuser, resulting in a shorter flow path. On the other hand, flow segregation caused by the three-hole probes is possible.

On the shroud side a spiral streamline is also evident (Fig. 37b). It is characterized by a different bending radius with respect to the hub side. This agrees with Krain's work [41], who observed slightly different velocity profiles on the hub and shroud close to the impeller

outlet. The absence of two flow trajectories, as showed on the hub side, is caused by the path of a liquid, which mainly affects the hub plane.

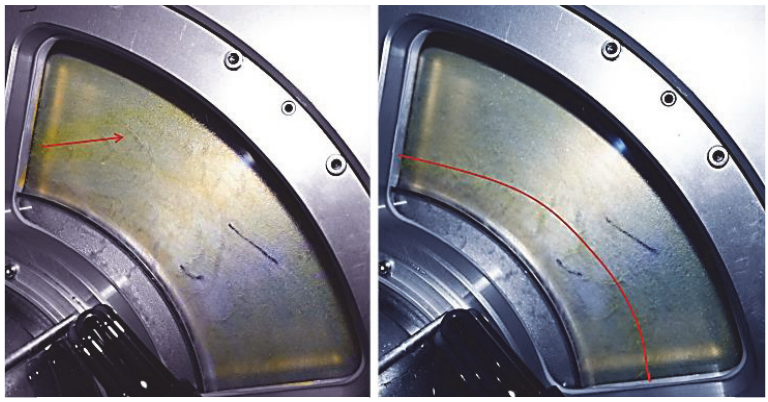

(a) (b)

Fig. 37: Diffuser inlet injection, 9000 rpm GMF 90% φ 0.065; (a) hub (b) shroud

The same trends are presented in Fig. 38, which refers to a flow coefficient equal to 0.04. Here the effects due to flow rate reduction are observable. Effective streamlines on both the hub and shroud have greater bending along the tangential direction. This means a longer flow path. When decreasing the flow coefficient and consequently the mass flow, a rise in the absolute angle and a drop of velocity radial component are registered. This effect is very clear on the hub, Fig. 38a.

On the shroud, Fig. 38b, the streamline has a perfect circular shape, completely surrounding the impeller exit. This proves that there is upcoming back flow from the impeller.

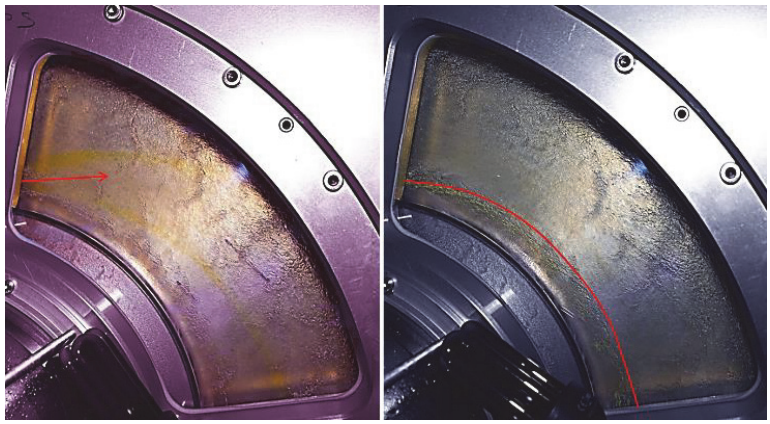

(a) (b)

Fig. 38: Diffuser inlet injection, 9000 rpm GMF 90% φ 0.04; (a) hub (b) shroud

The evolution of the flow path is presented in Fig. 39 for φ equal to 0.025. On the hub, Fig. 39a presents only one flow trajectory. The author asserts that this is a more radial streamline than that observed for φ equal to 0.04 as discussed above.

The disappearance of one streamline is considered to be the effect of the upcoming reverse flow, as already stated. So, result of flow unsteadiness, already visible in Fig. 38b, is revealed on the hub side too.

However, also on the shroud in Fig. 39b, the fluorescent fluid disappears nearly totally from the diffuser shroud. Therefore it is claimed that liquid doughnut at the impeller inlet, disclosed in Fig. 29, is partly “fed” by back flow from the diffuser.

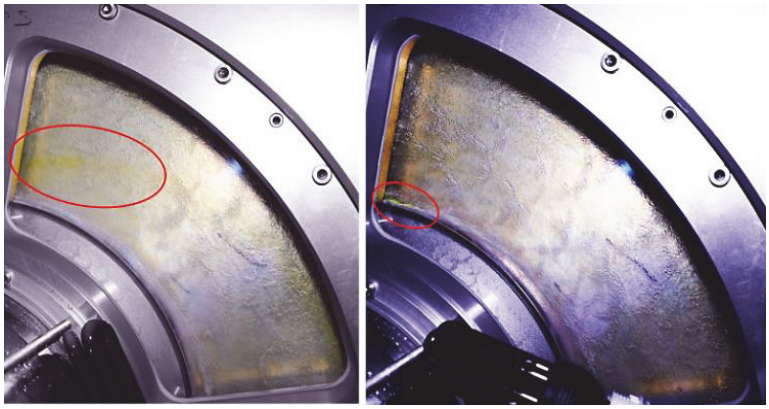

(a) (b)

Fig. 39: Diffuser inlet injection, 9000 rpm GMF 90% φ 0.025; (a) hub (b) shroud

This last indication is confirmed by analysing the evolution of the flow path at the diffuser outlet section in Fig. 40. By varying the flow coefficient, it is possible to see a shift of streamline towards the centre of the diffuser. This shows interaction between the diffuser and volute, suggesting that a reverse flow phenomenon occurs in the volute region, affecting the diffuser as well as the impeller.

An indication of instability evolution and development is given in the previous results, flow disturbance with the presence of the liquid phase moves from the shroud to hub sides in the diffuser region.

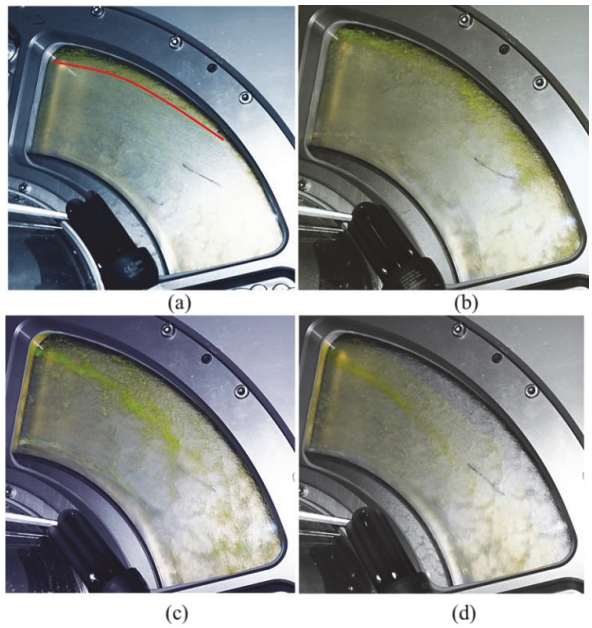

Fig. 40: Diffuser outlet injection, shroud side, 9000 rpm GMF 90%; (a) φ 0.065 (b) φ 0.04 (c) 0.03 (d) φ 0.025

The flow evolution in correspondence with the impeller inlet and diffuser section is documented approaching unstable operating conditions. The back flow mechanism is clearly detectable at the impeller tip area which involves the volute and diffuser too. Effectively a modification of diffuser streamlines testifies that reversal flow moves from the discharge scroll. Influence of fluid reduction is also evident in the jet patterns.

Left limit investigation

This section summarizes the results from the left limit investigation. An indication regarding the area explored during tests is shown in Fig. 41; the low mass flow region is analysed. The first part of the section deals with pressure trends during transient, followed by an examination of frequency analysis, supplemented by a comparison between dry and wet operations.

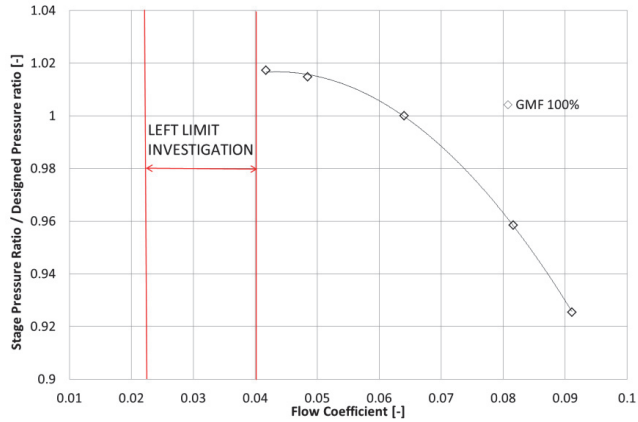

Fig. 41: Indication of area explored during left limit investigation

The left limit investigation has been realized by means of measurements from high-response dynamic pressure transmitters, in order to study the influence of the liquid phase on working range and identify characteristic frequencies of unsteadiness. The transient analysis was executed fixing a starting flow coefficient, which did not present any sub-synchronous phenomenon in the frequency spectrum, in general 0.04. The gas throttle valve was closed, reducing the flow coefficient and keeping a constant liquid flow rate. Anyway it is worth to noticing that the GMF value decreases accordingly to the flow coefficient, because the gas flow rate is reduced during transient.

The signal from dynamic pressure against time is plotted in Fig. 42. The graph presents the fluctuations in dynamic pressure relating to 6000 rpm and 92% of GMF; the unstable operating condition is included in the interval from 4 to 24 seconds. In this time interval, the valve position varies between 77 ($\varphi = 0.03$) and 87% ($\varphi = 0.0197$) of closure. After 24 s, the gain in pressure indicates restoration of normal compressor behaviour, because the initial position of the valve has been re-established.

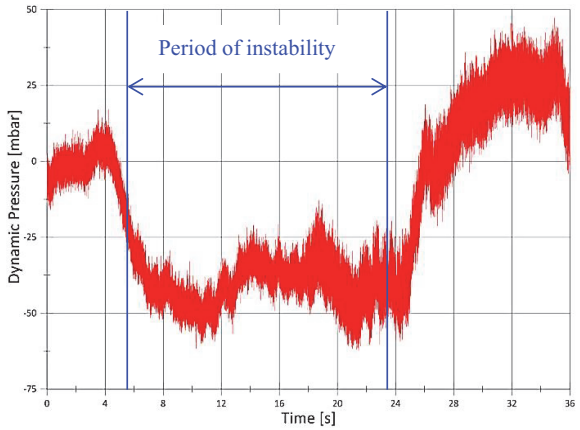

Fig. 42: Dynamic pressure signal in wet conditions, at 6000 rpm and GMF equal to 92%

Fig. 43 gives the static pressure ratio and flow coefficient against time. These data relate to a test in the presence of water at operating conditions of 6000 rpm and 92% of the GMF. It should be noted that the initial point, on the time line, is different from previous charts because they refer to a distinct acquisition file, even though the start conditions are identical in both cases. The pressure ratio reaches the minimum value in correspondence with a smaller value of φ, at about 64 s. As expected, a drop in pressure ratio is detected when moving towards surge. A complete doughnut formation is verified after approximately 34 seconds, in correspondence with a value of the flow coefficient equal to 0.0235. Unsteadiness therefore does not occur at the same moment as minimum pressure, which is reached during the restoration of the initial operating conditions.

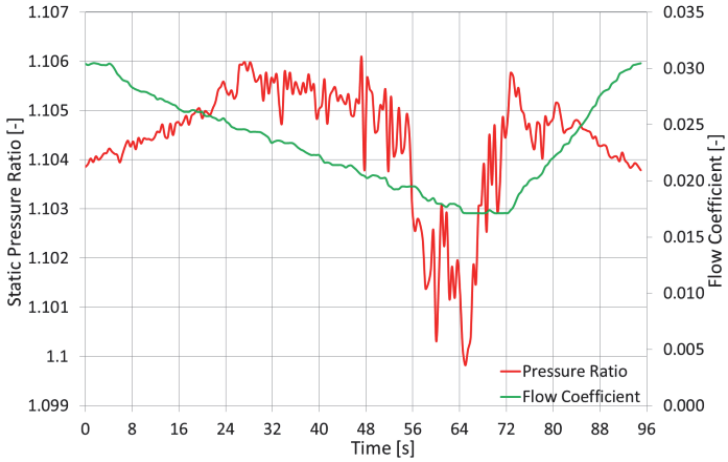

Fig. 43: Variation of static pressure ratio and flow coefficient over time approaching surge in wet conditions, at 6000 rpm and a GMF equal to 92%

A further clarification concerning this point is given in Fig. 44: the pressure ratio reaches the lowest value during the backflow period, just before opening the gas throttle valve. This graph is of specific interest because it presents a sort of hysteresis in instability owing to flow transition.

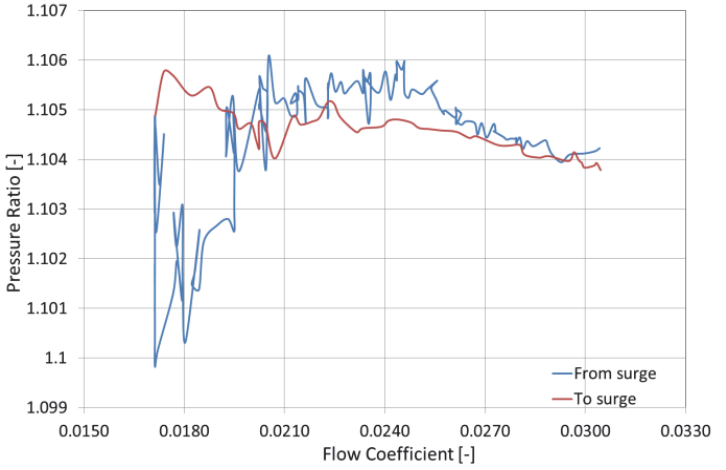

Fig. 44: Pressure ratio against flow coefficient in wet conditions, at 6000 rpm and a GMF equal to 92%

An evaluation of the pressure ratio trend against the flow coefficient is reported in Fig. 45 and Fig. 46, under dry and wet conditions, respectively. The graphs present an opposite slope: in dry the pressure ratio drops with the flow coefficient, while at 90% of GMF the PR increases when reducing the flow up to φ equal to 0.022, then it start to reduce.

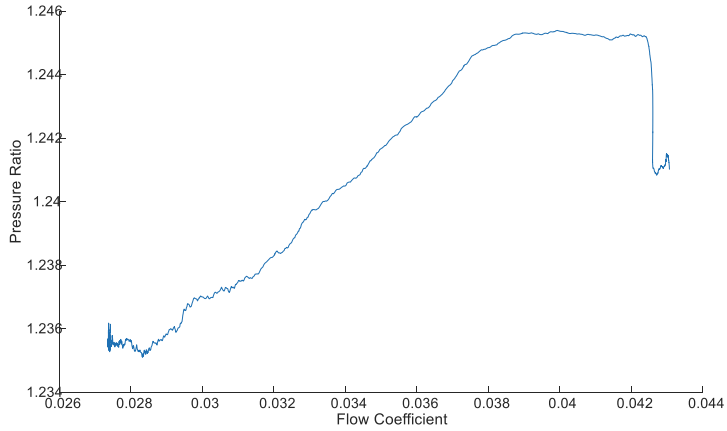

Fig. 45: Pressure ratio trend approaching surge in dry, at 9000 rpm

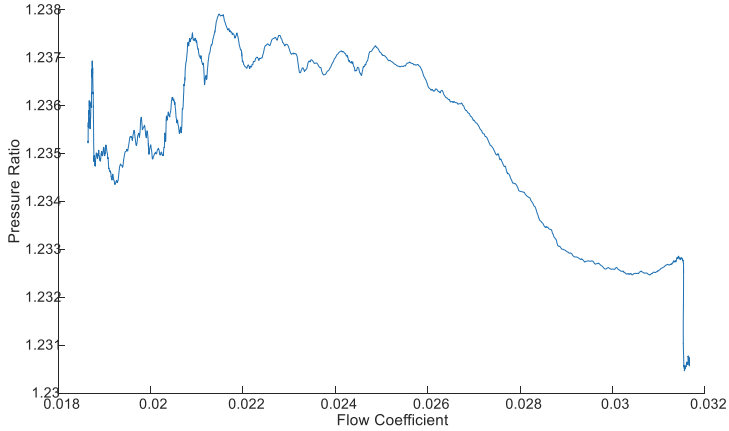

Fig. 46: Pressure ratio trend approaching surge with the presence of liquid, at 9000 rpm and 90% of GMF

Analysing the characteristic frequencies of these phenomena in detail and considering that the blade passing frequency is calculated as

$$BPF = \frac{RPM}{60} \cdot n°_{impeller\_blades}$$

at 9000 rpm the BPF is equal to 2550 Hz, as reported in Fig. 47. The graph presents a trend of frequencies at the design point for 9000 rpm and 90% of GMF; the blade passing frequency is clearly visible, besides the first harmonic, f_{1xrev}, around 150 Hz. No sign of instability is evident for φ 0.065 since no subsynchronous amplitude is prominent.

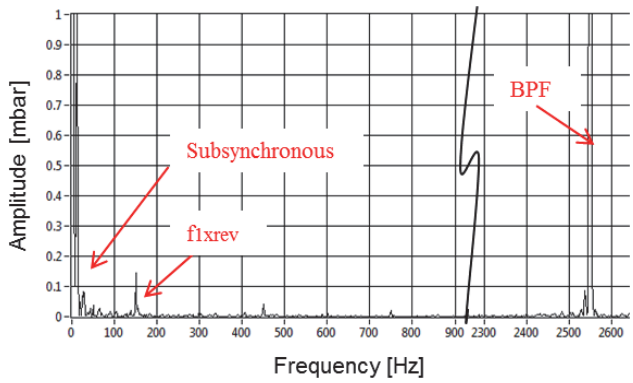

Fig. 47: FFT on diffuser inlet, 9000 rpm 90% GMF and φ 0.065

An instability indication appears for a flow coefficient equal to 0.03, in correspondence with the diffuser outlet section, as in Fig. 48b. The predominant subsynchronous amplitude is between 0.2 and 0.25 mbar, greater than the blade passing frequency, which is less than 0.15 mbar. This confirms unstable phenomena begin in the volute area.

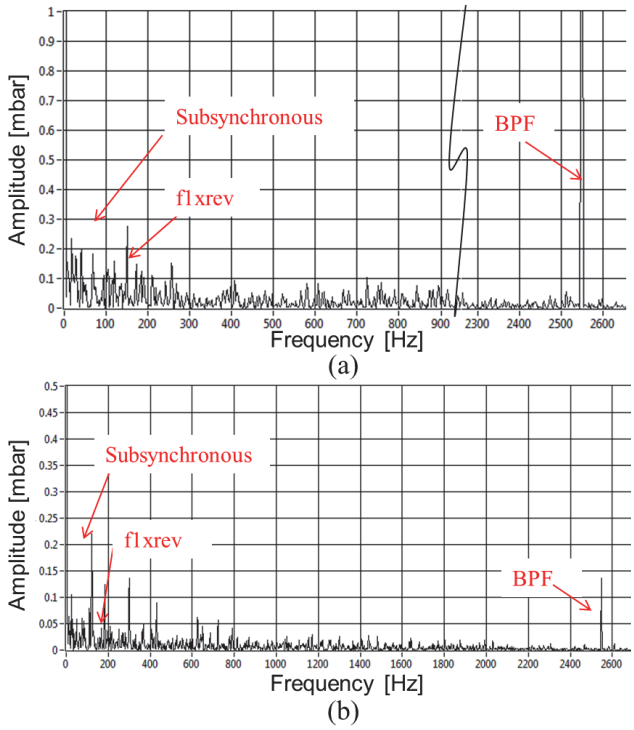

Fig. 48**:** FFT, 9000 rpm 90% GMF and φ 0.03, (a) diffuser inlet (b) diffuser outlet

It is useful to refer to a waterfall diagram, depicted in Fig. 50 and Fig. 51. In dry conditions the sub-synchronous term, at about 86 Hz, overtakes the blade passing frequency at φ equal to 0.034. Comparing the waterfall diagrams under dry and with a liquid amount equal to 90% of GMF (Fig. 50) almost the same frequency component is revealed. The main components vary linearly with the flow coefficient. In particular, the stall phenomenon

appears at approximately 35% of nominal flow. Under wet conditions, the instability appears at lower φ (0.023), with respect to the dry test (φ = 0.034), consequently the liquid presence is preventing the stall inception and does not limit the machine operating range. Increasing the amount of water, that is a reduction of gas mass fraction, stall tends to disappear. For 80% GMF (Fig. 51), the predominant components in correspondence with very low frequency can be detected, just before surge.

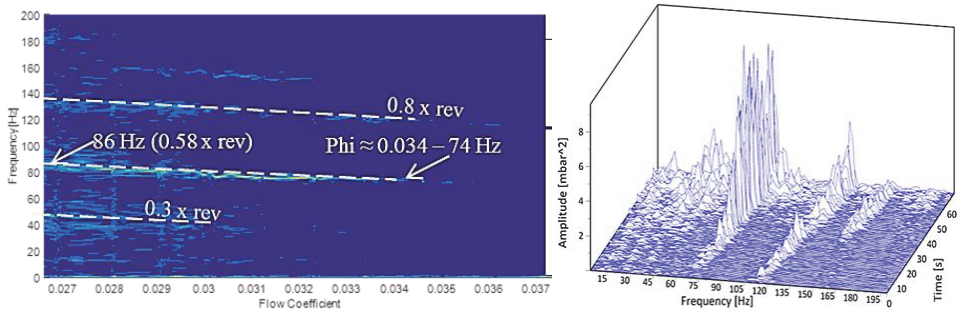

Fig. 49: Waterfall diagram, at 9000 rpm in dry conditions

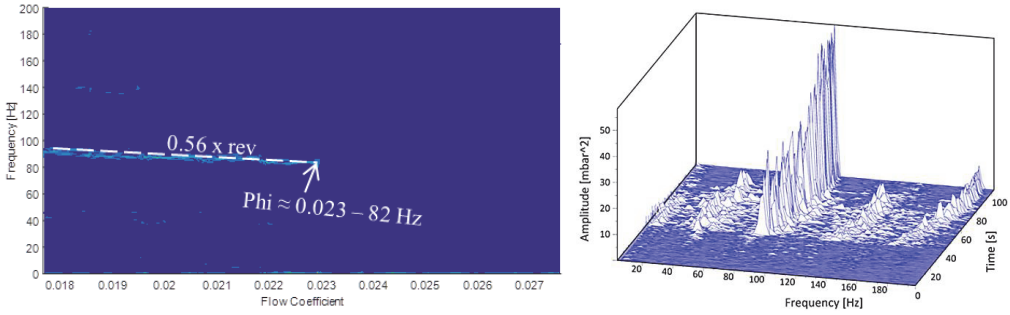

Fig. 50: Waterfall diagram, at 9000 rpm for 90% of GMF

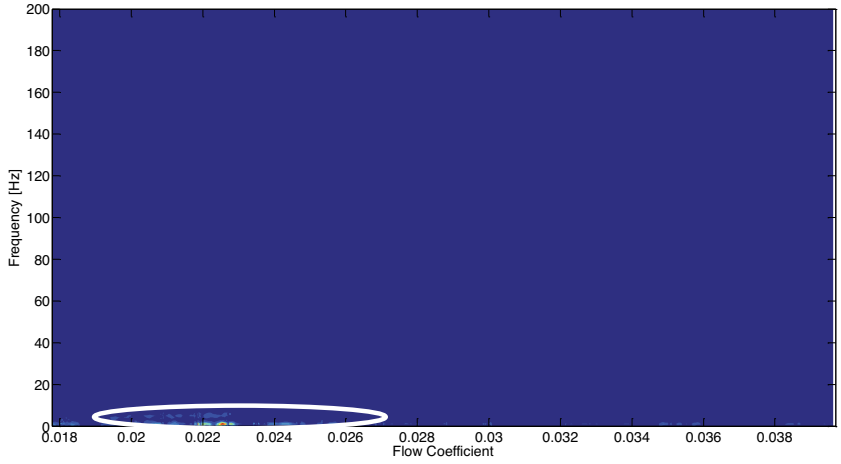

Fig. 51: Waterfall diagram, at 9000 rpm for 80% of GMF

A comparison of waterfalls calculated by signals from dynamic pressure probes is disclosed in Fig. 52. The spectrum graphs are related to the middle and discharge diffuser sections, respectively. Moreover Fig. 50 presents FFT diagram from transducer located in correspondence with inlet diffuser section. It should be noticed for each position that the same frequency components are revealed, around the BPF (180 Hz) and subsynchronous at 90, 50 and less than 10 Hz. The instability inception is observed at about 40 s as well, the peak amplitude decreases when moving from the inlet diffuser section.

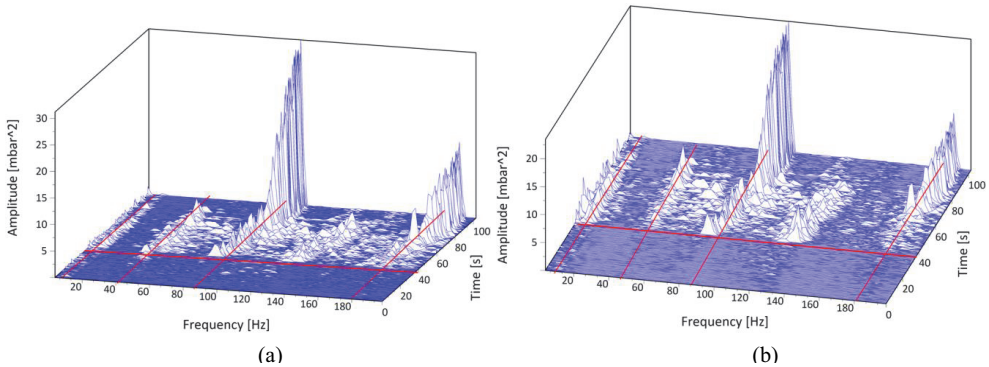

Fig. 52: Waterfall diagram, at 9000 rpm and 90% GMF. (a) Mid diffuser section; (b) Outlet diffuser section

So the left limit analysis confirms that the backflow under wet condition inside the diffuser, is produced on the shroud side because of flow segregation, as sketched in Fig. 53.

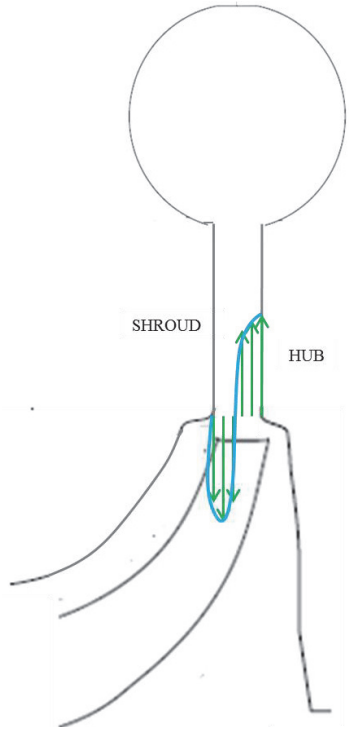

Fig. 53: Diffuser segregation when reversal flow occurs in wet condition

Erosion test

The erosion test results are illustrated below. The most significant images, taken during inspection, are reported for each step. After each stop of the compressor, all the blades and the channels have been checked in order to evaluate the erosion rate. The quality of painting is not good because the paint layer is not uniform. There is variation in the thickness of painting, in particular, many “wrinkles”, which modify the vane design are present. This is an indication about the qualitative information of the test.

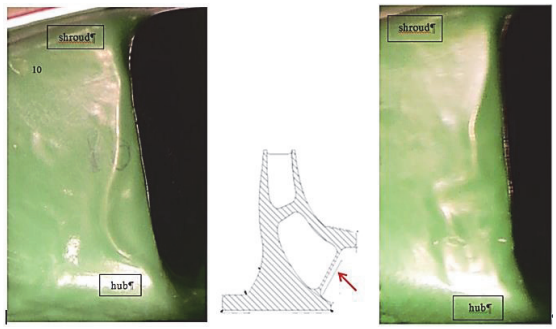

Fig. 54: Leading edge of two different blades after 30 min of erosion test

Fig. 54 shows the leading edge area after 30 minutes of erosion test. It is possible to see the paint is still intact, so the effects due to water are negligible. After 60 minutes of erosion test, in correspondence to leading edge, as shown in Fig. 55, the paint seems damaged close to the shroud

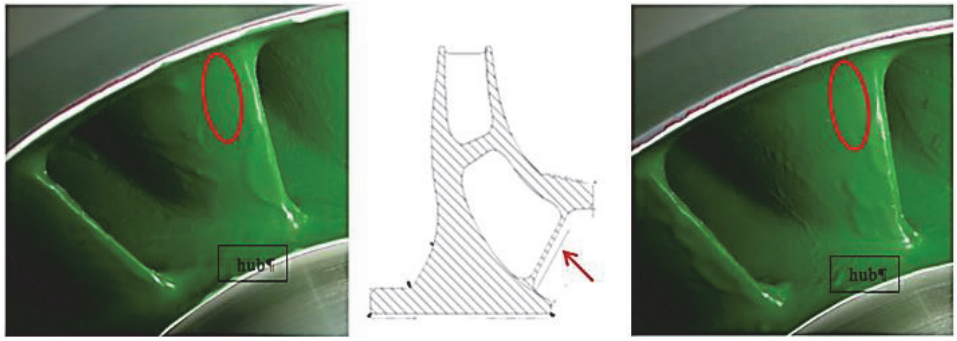

Fig. 55: Leading edge of two different blades after 60 min of erosion test

The action of water is more visible around the trailing edge area (see Fig. 56). On almost all the blades the detachment of all three layers of paint occurred at the same time. This phenomenon is probably caused by the lack of stickiness between primer and impeller surface and it is not brought about by erosion.

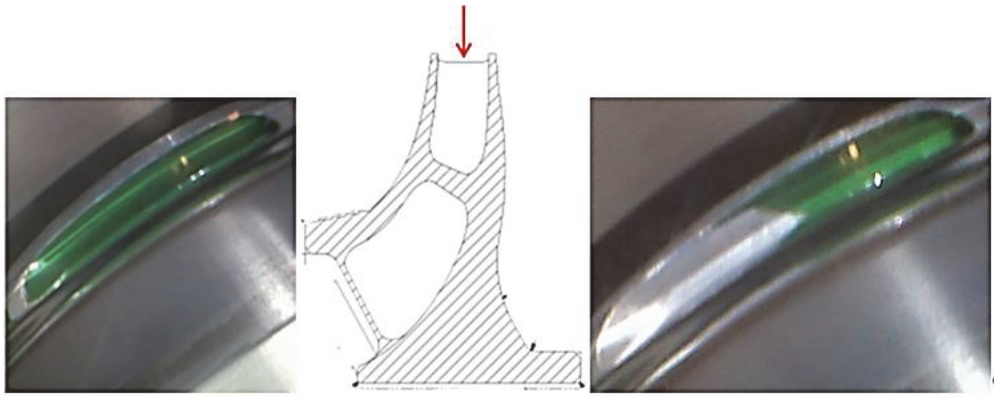

Fig. 56: Trailing edge of two different blades after 60 min of erosion test

Carrying on erosion test for 120 minutes, at leading edge (see Fig. 57) the green layer of paint is eroded, and, in consequence, little white points appear. Inside the channel, precisely in correspondence to the pressure side, as shown in Figure 12, some eroded regions appear in all blades

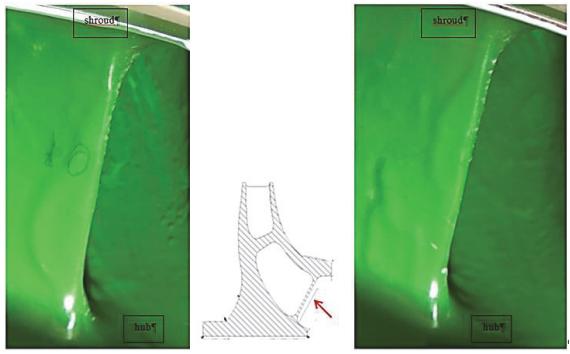

Fig. 57: Leading edge of two different blades after 120 min of erosion test

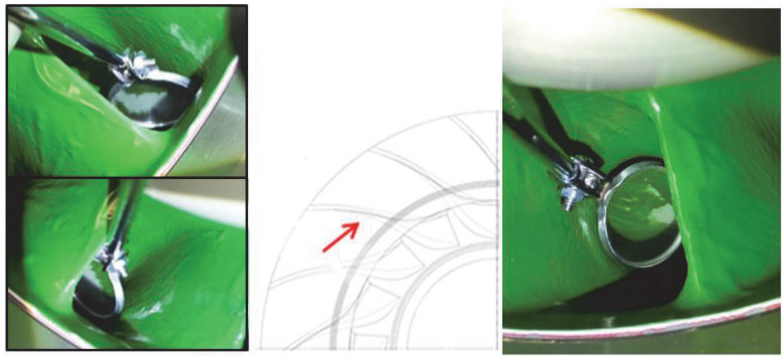

Fig. 58: Pressure side of two different blades after 120 min of erosion test

After 240 minutes of test (pictures are not given here), the erosion becomes deeper at the surface, exhibiting the little eroded points. This is larger compared to the condition at 120 minutes. Regarding the pressure side, larger areas of paint are worn away in comparison with

the condition after 120 minutes. Whereas, monitoring the trailing edge the variations in the eroded parts are not remarkable.

After six hours of erosion test, an unexpected situation appears, as shown in Fig. 59, on the suction side of blade, near to leading edge: a considerable part of paint moves away from the impeller, consequently it is decided to stop water injection, in order to avoid damage to the stator elements.

In Fig. 60, in correspondence to the trailing edge, the same phenomenon which affects the suction side can be noticed, as observed in Fig. 59.

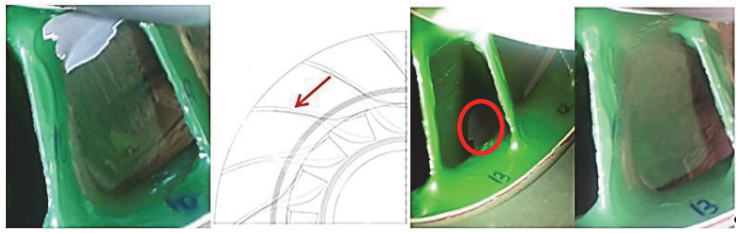

Fig. 59: Suction side of two different blades after 360 min of erosion test

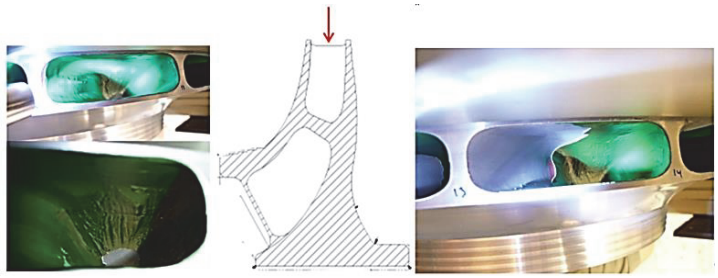

Fig. 60: Trailing edge of two different blades after 360 min of erosion test

From erosion test results it can be noticed after 30 minutes that there is no significant effect due to the action of water; the paint is undamaged, except in correspondence of the leading edge where some scratches appear. After one hour, mainly on the trailing edge, the coat sticks out form the surface of the impeller; this unexpected phenomenon is not attributed to erosion, but rather to the way in which the impeller was painted. The effect is amplified carrying on with erosion test, a gradual deterioration is documented. As a consequence of the paint leaving in the area close to hub, after six hours of erosion test, the water injection is stopped.

The erosion action is clearly visible after two hours of test, in correspondence to the leading edge and pressure side of each channel. In particular, on the leading edge, little white points can be noticed, while, on the pressure side, more large areas of the first paint layer have been eroded. Performing more tests, on the leading edge, the region affected by erosion becomes wider; the same trend occurs on the trailing edge, the eroded portion increases with time. In the first case, the erosion is more concentrated next to the shroud, because of the higher mix velocity, water and air. While inside the channel, the water drops hit the pressure side of the blade since they are not dragged along by air.

Conclusion

Four test campaigns have been performed on different research fields. The results are provided for each text matrix. The main outcomes were a unique view of wet inlet flow

instabilities under surge conditions: the fundamental mechanisms leading to annulus boundary blockage in correspondence with the inlet section and a reduction in the inlet flow area owing to the blockage and reverse flow are documented. Visualization of the diffuser path, evolving from design to off-design working conditions is documented, as well as flow interactions in the impeller/diffuser/volute regions. Reverse flow begins from the volute component, affecting both the diffuser and the impeller. Flow regime fluctuations and disturbance owing to instabilities are clearly observed on the diffuser shroud sides. No negative influence on stability and working range is detected.

5. Conclusion and recommendations for further work

The present research has been carried out on a single-stage centrifugal compressor, operating with the presence of a liquid phase. The main objective is to produce a consistent basis for understanding the behaviour of the machine under multiphase conditions, in particular, through performance tests, flow visualization and left limit investigation. Specific attention is focused on instabilities. Both stall and surge and their evolution have been central in this work in order to expose multiphase effects and the impact on the compressor stability and working range. This analysis represents vital input to improve the design and optimize a wet gas impeller stage as a solution for improving the mixing of the gas and liquid phase is required. In addition an important contribution from this work is how to detect an anti-surge method.

The first step is an evaluation of the stage performance, to assess the influence of the liquid phase on the behaviour of a standard three-dimensional impeller. Results establish deterioration in the mechanism in wet conditions. In effect a pressure ratio and efficiency reduction are determined with the presence of a liquid phase, owing to a high mixture (liquid-gas) density ratio. With particular regard to the total pressure ratio, no significant variation in respect to dry condition is observed operating with a small amount of liquid, 95% - 90% GMF. In overflow condition, a reduction of the operating range is detected when decreasing the gas mass fraction. On the other hand, an evident drop of the polytropic efficiency (12% losses at design point from fry to 95% of GFM) is marked under wet conditions. This phenomenon of performance degradation is certainly caused by a greater amount of mass flow with respect to dry operation that impacts on the density ratio. This suggests that efforts to optimize wet tolerant compressor components are necessary.

In analysing wet transient inlet flow in correspondence with the impeller eye section, the main outcome is the formation of a liquid doughnut when approaching surge. Effectively, reducing the flow coefficient, boundary layer separation along the tangential and axial direction is noticed. This generates a reduction in the flow area and a blockage of the inlet annulus section that produces a reverse flow from the impeller exit region. Further investigation about the influence of fluid leakage from impeller labyrinth seal show this mechanism is partly caused by liquid escape from the gap between the impeller and diffuser.

Studying the diffuser section reveals mainstream and secondary flow patterns, highlighting fluid interactions with the volute as well. Using a stroboscope lamp, jets are disclosed in correspondence with diffuser inlet area under wet conditions. Their development is observed reducing the mass flow rate. In particular, a clear indication of velocity flow evolution is given. At design flow and 90% of GMF a strong radial component is revealed, however with a lower and lower flow coefficient, a decrement in amplitude is observed. For a higher liquid content, i.e. 80% of gas mass fraction, a more significant tangential component is detected.

Diffuser streamlines testify that there is not a uniform flow in the diffuser width, moving from the shroud to the hub side great differences are marked. Investigation confirms the back flow starts on the shroud area of the diffuser. On the other hand, the typical spiral path is documented. It should be noted at off-design conditions a longer logarithmic path in respect to best point is verified. Moreover an indication of back flow is given. In particular, an

indication that this phenomenon originates from the volute is specified. Additionally, flow reversal begins from the diffuser shroud side.

Regarding the working range, fast Fourier transform analysis confirms that the presence of a liquid phase has a stabilizing effect on the unsteadiness onset. In respect to dry conditions, indication of instability in wet operation appears at a lower flow coefficient, so the left side of the compressor range is not negatively affected by the liquid amount. A peculiarity emerges at low GMF, e.g. 20%, since stall phenomena completely disappear, while evidence of surge still persists.

In order to analyse the instability onset inside the diffuser, it is useful to install high-response dynamic pressure sensors in different tangential and axial positions. In this way, a complete overview of the unsteady phenomenon will be given. Moreover it will be interesting to evaluate the effect of different inlet conditions on the performance; in particular the influence of droplet size on the pressure ratio can be documented and diverse inlet flow regimes can be explored.

References

[1] M. P. Boyce, Centrifugal Compressors: A Basic Guide, PennWell, 2003

[2] G. O. Musgrove, M. A. Poerner and M. Bertoneri, "Overview of Important Considerations in Wet Gas Compression Testing and Analysis," in *43rd Turbomachinery & 30th Pump Users Symposia*, 2014.

[3] M. P. Boyce, Gas Turbine Engineering Handbook, 4th Edition, Elsevier Inc., 2012.

[4] R. C. Dean and Y. Senoo, "Rotating Wakes in Vaneless Diffuser," *Trans. ASME J. of Basic Eng.,* vol. 82, pp. 563-74, 1960.

[5] D. Eckardt, "Detailed Flow Investigation Whitin a High-Speed Centrifugal Compressor Impeller," *Trans. ASME J. of Fluids Eng.,* vol. 98, pp. 390-402, 1976.

[6] H. Krain, "Swirling Impeller Flow," *Trans. of ASME J. of Turbomach.,* vol. 110, pp. 122-8, 1988.

[7] M. W. Johnson and J. Moore, "Secondary Flow Mixing Losses in a Centrifugal Impeller," *Trans. ASME J. of Eng. Power ,* vol. 105, pp. 24-32, 1982.

[8] N. A. Cumpsty, Compressor Aerodynamics, Krieger Publishing Company, 2004.

[9] O. Dubitisky and D. Japiske, "Vaneless Diffuser Advanced Model," *J. of Turbomach.,* vol. 130, 2008.

[10] M. Inoue, "Radial Vaneless Diffusers: A Re-Examination of the Theories of Dean and Senoo and of Johnston and Dean," *Trans. ASME J. of Fluid Eng.,* vol. 105, pp. 21-7, 1983.

[11] Y. K. P. Shum, C. S. Tan and N. A. Cumpsty, "Impeller-Diffuser Interaction in a Centrifugal Compressor," *Trans. ASME J. of Turbomach.,* vol. 122, pp. 777-86, 2000.

[12] D. Hagelstein, K. Hillewaert, R. A. Van den Braembussche, R. Keiper, M. Rautenberg and A. Engeda, "Experimental and NUmerical Investigation of the Flow in a Centrifugal Compressor Volute," *Trans. of ASME,* vol. 122, pp. 22-31, 2000.

[13] S. Khalfallah and A. Ghenaiet, "Analysis of Impeller-Vaneless-Diffuser-Scroll Interactions in a Radial Compressor," *J. Power and Energy,* vol. 224, pp. 851-67, 2010.

[14] R. C. Pampreen, Compressor Surge and Stall, Concepts ETI, Inc., 1993.

[15] I. J. Day, "Stall, Surge and 75 Years of Research," in *ASME Turbo Expo, GT2015-44109*, 2015.

[16] E. Lennemann and J. H. G. Howard, "Unsteady Flow Phenomena in Rotating Centrifugal Impeller Passages," *J. of Eng. for Power,* pp. 65-71, 1970.

[17] P. Frigne and R. Van Den Bræmbussche, "Distinction Between Different Types of Impeller and Diffuser Rotating Stall in a Centrifugal Compressor With Vaneless Diffuser," *Trans. of ASME,* vol. 106, pp. 468-474, 1984.

[18] W. Jansen, "Rotating Stall in a Radial Vaneless Diffuser," *Trans. of ASME,* pp. 750-758, 1964.

[19] Y. Senoo and Y. Kinoshita, "Limits of Rotating Stall and Stall in Vaneless Diffuser of Centrifugal Compressors," in *Gas Turbine Conference, 78-GT-19*, 1978.

[20] M. J. Sorokes, J. E. Pacheco, C. Vezier and S. Fakhri, "An Analytical and Experimental Assessment of a

Diffuser Flow Phenomenon as a Precursor to Stall," in *ASME Turbo Expo, GT2012-69122*, 2012.

[21] K. Toyama, P. W. Runstadler and R. C. Dean, "An Experimental Study of Surge in Centrifugal Compressors," *J. of Fluids Eng.,* pp. 115-124, 1977.

[22] D. N. Gonzàlez , J. P. M. Smeuers and L. Tapinassi, "Predictability of Rotating Stall and Surge in a Centrifugal Compressor Stage with Dynamic Simulations," in *ASME Turbo Expo, GT2014-26712*, 2014.

[23] J-S. Kang and S-H. Kang, "Stall Inception in a High Speed Centrifugal Compressor," in *ASME Turbo Expo, GT2001-0301*, 2001.

[24] A. X. Liu and X. Q. Zheng, "Methods of Surge Point Judgment for Compressor Experiments," *Experimental Thermal and Fuid Science,* vol. 51, pp. 204-213, 2013.

[25] A. Bianchini, D. Biliotti, M. Giachi, E. Belardini, L. Tapinassi, L. Ferrari and G. Ferrara, "Some guidelines For the Experimental Characterization of Vaneless Diffuser Rotating Stall In Stages of industrial Centrifugal Compressor," in *ASME Turbo Expo, GT2014-26401*, 2014.

[26] N. Aretakis , K. Mathioudakis , M. Kefalakis and K. Papailiou , "Turbocharger Unstable Operation Diagnosis Using Vibroacoustic Measurements," *ASME J. of Eng. for Gas Turbine Power,* vol. 126, pp. 840-847, 2004.

[27] M. Morini , M. Pinelli and M. Venturini, "Acoustic and Vibrational Analyses on a Multi-Stage Compressor for Unstable Behavior Precursor Identification," in *ASME Turbo Expo, GT2007-27040*, 2007.

[28] I. Day , J. Williams and C. Freeman, "Rain Ingestion in Axial Flow Compressors at Part Speed," in *ASME Turbo Expo, GT2005-68582*, 2005.

[29] I. Roumeliotis and K. Mathioudakis, "Water Injection Effects on Compressor Stage Performance," in *ASME Turbo Expo, GT2006-90427*, 2006.

[30] L. Minghong and Z. Qun, "Wet Compression System Stability Analysis Part I," in *ASME Turbo Expo, GT2004-54020*, 2004.

[31] Z. Qun and L. Minghong, "Wet Compression System Stability Analysis Part II," in *ASME Turbo Expo, GT2004-54020*, 2004.

[32] T. G. Grüner and L. E. Bakken, "Instability Characteristic of a Single-stage Centrifugal Compressor Exposed to Dry and Wet Gas," in *ASME Turbo Expo, GT2012-69473*, 2012.

[33] Ø. Hundseid, "Evaluation of Performance Models for Wet Gas Compressors," Norwegian University of Science and Technlogy, PhD Thesis, 2008.

[34] L. Brenne, T. Bjørge, J. L. Gilarranz, J. M. Koch and H. Miller, "Performance Evaluation of a Centrifugal Compressor Operating Under Wet Gas Conditions," in *34th Turbomachinery & 21th Pump Users Symposia*, 2005.

[35] M. Fabbrizzi, C. Cerretelli, F. Del Medico and M. D'Orazio, "An Experimental Investigation of a Single Stage Wet Gas Centrifugal Compressor," in *ASME Turbo Expo, GT2009-59548*, 2009.

[36] M. Bertoneri, S. Duni, D. Ransom, L. Podestà, M. Camatti, M. Bigi and M. Wilcox, "Measured Performance of Two-Stage Centrifugal Compressor Under Wet Gas Conditions," in *ASME Turbo Expo, GT2012-69473*, 2012.

[37] T. G. Grüner and L. E. Bakken, "Wet Gas Impeller Test Facility," in *ASME Turbo Expo, GT2010-22618*, 2010.

[38] L. Brenne, “Straight-Walled Diffuser Performance,” Norwegian University of Science and Technology, PhD Thesis, 2004.

[39] Ø. Hundseid, L. E. Bakken, T. G. Grüner, L. Brenne and T. Bjørge, “Wet Gas Compression on a Single Stage Centrifugal Compressor,” in *ASME Turbo Expo, GT2008-51156,* 2008

[40] Ø. Hundseid and L. E. Bakken, “Integrated Wet Gas Compressor Test Facility,” in *ASME Turbo Expo, GT2015-43004*, 2015.

[41] H. Krain, “A Study on Centrifugal Impeller and Diffuser Flow,” *Trans. of ASME,* vol. 103, pp. 699-697, 1981.

Appendix

PAPER I

Is not included due to copyright

PAPER II

Is not included due to copyright

PAPER III

Is not included due to copyright

PAPER IV

Is not included due to copyright